Early downregulation of HC-specific genes in the vestibular sensory epithelium during chronic ototoxicity

Borrajo, Mireia[1,2,3]*; Greguske, Erin A. [1,2,3] *; Maroto, Alberto F.[1,2,3]*; Palou, Aïda[1,2,3]*; Giménez-Esbrí, Víctor[1]; Sedano, David[1]; Gut, Marta[4,5]; Esteve-Codina, Anna[4,5]; Martín-Mur, Beatriz[4,5]; Barrallo-Gimeno, Alejandro[1,2,3]; Llorens, Jordi[1,2,3]

*: M.B., E.A.G., A.F.M. and A.P. are equal first authors.

[1] Departament de Ciències Fisiològiques, Universitat de Barcelona, Hospitalet de Llobregat, Catalunya, Spain
[2] Institut de Neurociències, Universitat de Barcelona, Barcelona, Catalunya, Spain
[3] Institut d'Investigació Biomèdica de Bellvitge (IDIBELL), Hospitalet de Llobregat, Catalunya, Spain
[4] CNAG-CRG, Centre for Genomic Regulation, Barcelona Institute of Science and Technology (BIST), Barcelona, Spain.
[5] Universitat Pompeu Fabra, Barcelona, Spain.

e-Mail addresses and ORCID codes

M.B.: mborrajoarjona@ub.edu; 0000-0003-2126-5713
E.A.G.: greguske.e@gmail.com; 0000-0001-8536-7669
A.F.M.: albertomaroto@hotmail.com; 0000-0001-8265-4902
A.P.: apaloumi45@ub.edu; 0000-0002-5252-6245
V.G.-E.: vgimenezes@uic.es; 0000-0001-5294-0158
D.S.: dsflash7@gmail.com; 0009-0008-5114-9784
M.G.: marta.gut@cnag.eu; 0000-0002-4063-7159
A.E.C.: anna.esteve@cnag.eu; 0000-0003-0361-2873
B.M.-M.: beatriz.martin@cnag.eu; 0000-0002-6006-3295
A.B.G.: abarrallo@ub.edu; 0000-0003-2086-8926
J.L.: jllorens@ub.edu; 0000-0002-3894-9401

Acknowledgements:

The confocal microscopy studies were performed at the Centres Científics i Tecnològics de la Universitat de Barcelona (CCiTUB). We thank Dr. Benjamín Torrejon-Escribano and Dr. Ashraf Muhaisen for their expert and technical help, and students Clara López Escolà, Javier Domínguez Rovira, Júlia Valor Blanquer and Maria Capdevila Bayo for their contributions towards the studies. We also thank Dr. Ana Lysakowsi for advice on KCNA10 labelling.

Funding:

This research was supported by Ministerio de Ciencia, Innovación y Universidades, Agencia Estatal de Investigación, MCIU/AEI, 10.13039/501100011033, and European Regional Development Fund, FEDER, grant numbers RTI2018-096452B-I00 and PID2021-124678OB-I00. A.B.G is a Serra-Húnter fellow (Generalitat de Catalunya). E.A.G. was supported by the Ajuts per a la contractació de personal investigador predoctoral en formació (FI-AGAUR) program (Generalitat de Catalunya). M.B. and E.A.G. were supported by the Formación del Profesorado Universitario (FPU) program (Ministerio de Universidades).

ABSTRACT

Exposure of mammals to ototoxic compounds causes hair cell (HC) loss in the vestibular sensory epithelia of the inner ear. In chronic exposure models, this loss often occurs by extrusion of the HC from the sensory epithelium towards the luminal cavity. HC extrusion is preceded by several steps that begin by detachment and synaptic uncoupling of the cells from the afferent terminals of their postsynaptic vestibular ganglion neurons. To identify gene expression programs driving these responses to chronic ototoxic stress, we performed five RNA-seq control versus treated comparisons involving two species (rat and mouse), two compounds (streptomycin and 3,3'-iminodipropionitrile, IDPN), and three time points in the rat/IDPN model. By comparing the differentially expressed genes and their associated Gene Ontology terms, we identified both common and model-unique expression responses. The earliest and most robust common response was a downregulation of HC-specific genes, including stereocilium (*Atp2b2, Xirp2*), synaptic (Nsg2), and ion channel genes (*Kcnab1*, *Kcna10*), together with new potential biomarkers of HC stress (*Vsig10l2*). This response was validated by in-situ hybridisation and immunofluorescence analyses. A second common response across species and compounds was the upregulation of the stress mediator *Atf3*. Model- or time- restricted responses included downregulation of cell-cell adhesion and mitochondrial ATP synthesis genes, and upregulation of interferon response, unfolded protein response and tRNA aminoacylation genes. The present results provide key insights on the responses of the vestibular sensory epithelium to chronic ototoxic stress, potentially relevant to other types of chronic stress.

KEYWORDS: Ototoxicity; 3,3'-iminodipropionitrile (IDPN); streptomycin; vestibular sensory epithelium; rat; mouse; RNA-seq; hair cell.

INTRODUCTION

The vestibular system in the inner ear, also known as labyrinth, is a sensor of head accelerations. The cells responsible for sensory transduction are known as hair cells (HC) due to the bundle of filiform extensions, named stereocilia, that they have at their apical end. Stereocilia bundles protrude into the endolymph-filled luminal cavities of the labyrinth and express the molecular mechanisms that trigger depolarization or hyperpolarization of the cells in response to their deflection by acceleration forces. In mammals, the HCs are organized in five sensory epithelia per ear: one utricle, one saccule, and three cristae. There are two types of HC, type I (HCI) and type II (HCII), which can be differentiated by morphological, molecular, and physiological criteria (Eatock and Songer, 2011; McInturff et al., 2018) . The most prominent differential feature is the calyx terminal, a unique afferent formation that encases HCIs but not HCIIs. These two types include several subtypes. For instance, both HCIs and HCIIs may or may not express the calcium-binding protein oncomodulin (Hoffman et al., 2018) and HCIs may or may not be encased by calyces expressing another calcium-binding protein, calretinin (Lysakowski et al., 2011).

Vestibular HCs and the related auditory HCs of the cochlea are damaged by several toxic molecules, therefore named ototoxic compounds. These include aminoglycoside antibiotics (streptomycin, gentamicin, and others), the chemotherapeutic agent cisplatin, and several low molecular weight nitriles (3,3'-iminodipropionitrile - IDPN, *cis*-crotonitrile, allylnitrile) (Boyes et al., 2020). Human therapeutic use or animal experimental exposure to these ototoxic compounds cause HC loss resulting in permanent vestibular and auditory deficits, as HCs do not regenerate in mammals or only to a very limited, non-functional, extent. The molecular processes leading to HC loss have been the subject of intense research, mostly in the hope that their understanding could reveal targets for prophylactic drugs that could prevent the permanent loss of function that may occur after use of the ototoxic agents. Most of the research has focused on ototoxic-induced HC apoptosis (Furness 2015). However, HCs can respond to injury stimuli by extrusion, a process by which the HC modifies its ultrastructural features and is ejected as a live cell from the sensory epithelium towards the vestibular luminal cavity. This is followed by degeneration of the ejected cell in the lumen. Cell extrusion is a form of cell demise that can only operate in epithelia. It has been identified as the main process of HC demise in the inner ear of birds and amphibians (Hirose et al., 1999; Rubel et al., 2013) and has been occasionally observed in the mammalian inner ear after ototoxicity (Li et al., 1995; Nakagawa et al., 1997; Granados and Meza, 2005), but it has been scarcely studied. Recent evidence indicates that retinal photoreceptor cells may also suffer extrusion (Völkner et al., 2022). Previous research in our laboratory identified a model, chronic exposure of rats to IDPN, in which most or all of the vestibular HCs are eliminated by extrusion (Seoane et al., 2001a,b). Subsequent research in rats (Sedó-Cabezón et al., 2015) and mice (Greguske et al., 2019) revealed that during IDPN intoxication the extrusion process is preceded by a reversible uncoupling of the HC and their post-synaptic afferents. A major hallmark of this process is the dismantlement of the calyceal junction, a cell-adhesion and signalling complex that is normally formed between the HCI and its corresponding calyx. This is paralleled by a major loss of vestibular function (Sedó-Cabezón et al., 2015; Greguske et al., 2019; Martins-Lopes et al., 2019; Schenberg et al., 2023). If the intoxication continues, stereocillia start to fuse and HCs are driven toward extrusion to irreversible loss (Llorens and Rodríguez-Farré, 1997; Seoane et al. 2001a, b). However, if the intoxication is terminated before stereocilia fusion begins, the calyx junction, synaptic, and behavioural defects are reversed (Sedó-Cabezón et al., 2015; Greguske et al., 2019; Martins-Lopes et al., 2019; Schenberg et al., 2023). Recently, we have collected evidence that calyx junction dismantlement also precedes HC extrusion in rats exposed to chronic streptomycin and may also occur in response to other sources of stress, such as that caused in human vestibular epithelia by a neighbouring vestibular schwannoma (Maroto et al., 2023).

The observations above suggest that extrusion is a process of regulated cell demise alternative to apoptosis. The genetically programmed process that executes apoptosis has been extensively characterized (Vitale et al., 2023), but the program driving HC extrusion has yet to be studied. Our observations that extrusion may be a slow

process that begins by reversible steps make this study a particularly interesting one, as this opens windows for pharmacological intervention to halt damage progression or accelerate repair. The present study is a first approach to the discovery of molecular mechanisms involved in vestibular sensory epithelium damage during chronic ototoxicity leading to HC extrusion. We hypothesized that these mechanisms would include specific gene expression signatures even though mechanisms other than gene expression modifications must be involved in the execution of the cell extrusion. We also hypothesized that the more important gene expression changes would be more conserved across evolution and more consistently triggered by different ototoxic compounds. Therefore, we performed RNAseq studies in chronic ototoxicity models involving two different species (mouse and rat) and two ototoxic compounds (IDPN and streptomycin). We also evaluated different time points in one of the models. As the objective was to understand the response to a slowly evolving stress condition, we hypothesized that the stress caused by cell isolation protocols, as those necessary for single-cell or purified cell population studies, would mask the gene expression changes of interest. Therefore, we used whole tissue for RNA extraction and sequencing. The results show similar and dissimilar changes in gene expression in the different models. Among these, the earliest common response in all ototoxicity models is a decreased expression of many HC-specific genes, associated with decreased expression of the corresponding proteins as shown by follow-up studies. In addition, other common and model-unique responses to chronic ototoxicity were also identified.

MATERIALS AND METHODS

Animals and treatments

The use of animals followed the local regulations (Law 5/1995 and Act 214/1997 of the Generalitat de Catalunya, and Law 6/2013 and Act 53/2013 of the Gobierno de España) in agreement with the EU Directive 2010/63. The experimental protocols were approved by the Universitat de Barcelona's Ethics Committee on Animal Experiments and the Commission on Animal Experimentation of the Generalitat de Catalunya. We used both Long-Evans rats, obtained from Janvier Labs (Le-Genest-Saint-Isle, France), and 129S1/SvImJ mice from a locally established colony, descendants of animals purchased from Jackson Laboratory (Bar Harbor, ME, USA). In all experiments, animals were housed in Macrolon cages in groups of at least 2 subjects with wood shavings as bedding. The housing conditions were standard, including a 12:12 h light:dark cycle (07:30-19:30 h), a 22±2°C room temperature and an *ad libitum* access to standard diet pellets (TEKLAD 2014, Harlan Laboratories, Sant Feliu de Codines, Spain).

Four experiments were carried out. In all of them, the animals were euthanized for tissue collection on the last day of treatment. We used exposure conditions causing progressive vestibular damage as thoroughly described in previous reports (Sedó-Cabezón et al., 2015; Greguske et al., 2019; Maroto et al., 2023). In three experiments we selected doses and times of exposure causing the maximum possible but still reversible vestibular function loss after IDPN in mice and rats, and after streptomycin in rats. Thus, in the first experiment, 2- to 4-month-old male 129S1/SvImJ mice were provided free access to water spiked with 0 (Control) or 30 (mouse/IDPN) mM of IDPN (>98%, TCI Europe, Zwijndrecht, Belgium) as the sole source of drinking liquid for 8 weeks. In the second experiment, male adult Long-Evans rats (8-9 weeks old on reception) were given 0 (Control) or 20 (rat/IDPN-4wk) mM of IDPN for 4 weeks. For the third experiment, male and female rats were obtained at post-natal day 8-9 and housed with their lactating mothers until weaning at day 21. Starting that day, the rats in the streptomycin group (rat/STREP) received streptomycin sulphate salt (Sigma-Aldrich, S6501), s.c., dissolved in phosphate-buffered saline (PBS), once a day for 6 weeks, at 500 mg/kg day (as free base). Control rats were injected with PBS. Initial injection volumes were 10 ml/kg to guarantee dose accuracy but were reduced to 2 ml/kg as the rats gained weight. The injection site in the dorsal skin was changed from day to day. Finally, another rat/IDPN experiment was added to obtain data on an earlier step of the HC detachment (Sedó-Cabezón

et al., 2015) or on a later time point when stereocilia fusion indicates the beginning of the active HC extrusion (Seoane et al., 2001a; Sedó-Cabezón et al., 2015). In this fourth experiment, the 20 mM concentration was used for 3 weeks (rat/IDPN-3wk) or 7 weeks (rat/IDPN-7wk) and a single control group included animals euthanized at each time point.

Assessment of vestibular function

To evaluate vestibular function in rats, we assessed the tail-lift reflex. Briefly, rats are held by the base of the tail and quickly but gently lifted upwards to approximately 40 cm above ground and immediately returned down. In healthy rats, this triggers a trunk and limb extension reflex in a landing response. Loss of vestibular function results in loss of this anti-gravity extension reflex, so the rat curls ventrally. The reflex response is recorded with high-speed video and the movie is used to determine the tail-lift angle (TLA), where the minimum angle is drawn by the nose, the back of the neck, and to the base of the tail during the tail-lift manoeuvre, as described (Martins-Lopes et al., 2019; Maroto et al., 2021 a,c).

In mice, loss of vestibular function was assessed using a previously validated behavioural test battery (Soler-Martín et al., 2007; Saldaña-Ruíz et al., 2013; Greguske et al., 2019; Maroto et al., 2021c). Briefly, mice are blindly rated 0 to 4 on 6 items. The ratings are 0 for the behaviours characterizing normal healthy animals and 4 for the maximal possible deviation from the normal behaviour. The mice are placed for one minute in a clean open arena, and rated for circling (stereotyped circulatory ambulation), retropulsion (backward movement), and abnormal head movements (intermittent extreme backward extension of the neck). Afterwards, the animals are rated for the tail-lift reflex, the contact inhibition of the righting reflex, and the air-righting reflex. More detailed descriptions of the battery are available (Saldaña-Ruiz et al., 2013; Greguske et al., 2019; Maroto et al., 2021c). Although the tail-lift reflex included in the mouse test battery is the same reflex used to assess vestibular dysfunction in rats, a protocol for reliable quantification of this reflex has not been validated in mice yet.

Sample collection

At the end of the exposure periods, 5-6 animals per group were decapitated and their vestibular epithelia quickly dissected in ice-cold PBS for RNA isolation. From each animal, the six cristae and the two utricles were isolated, cleaned of adjacent tissues, pooled, placed in an Eppendorf tube, frozen in liquid nitrogen, and stored at -80ºC. After RNA isolation and quality control as described below, three samples per group were used for RNA-seq. Thus, the mouse/IDPN, rat/IDPN-4wk, and rat/STREP experiments compared 3 control and 3 treated animals. In the streptomycin experiment, both the control and treated groups were composed of two male and one female rats. The other rat/IDPN experiment compared 3 control rats, 3 rats exposed to IDPN for 3 weeks, and 3 rats exposed to IDPN for 7 weeks.

For immunofluorescence and RNA-scope studies, the vestibular epithelia were quickly dissected in cold 4% paraformaldehyde in PBS under a fume hood, fixed in the same solution for 1 h, transferred into a cryo-preservative solution (34.5% glycerol, 30% ethylene glycol, 20% PBS, 15.5% distilled water) and stored at -20ºC. The present experiments were carried out using new samples as well as archival samples from previous studies (Sedó-Cabezón et al., 2015; Greguske et al., 2019; Maroto et al., 2023) stored for up to 10 years. For each analysis, we used sensory epithelia from control and treated animals that had been obtained at the same time.

Short read, low-input RNA sequencing

Total RNA was extracted from these samples using the Qiagen RNeasy mini kit and the manufacturer's protocol. RNA sequencing libraries were prepared following the SMARTseq2 protocol (Picelli et al., 2013) with some modifications. Briefly, the total RNA samples were quantified by Qubit® RNA BR Assay kit (Thermo Fisher Scientific) and the RNA integrity was estimated with an Agilent RNA 6000 Pico Bioanalyzer 2100 Assay (Agilent). Reverse transcription of the total RNA input material of 1.8 µl (6-11 ng, in function of the sample availability)

was performed using SuperScrpit II (Invitrogen) in the presence of oligo-dT30VN (1µM; 5'-AAG CAG TGG TAT CAA CGC AGA GTA CT30VN-3'), template-switching oligonucleotides (1 µM) and betaine (1M). The cDNA was amplified using the KAPA Hifi Hotstart ReadyMix (2x) (Roche) and 100 nM IS PCR primer (5'-AAG CAG TGG TAT CAA CGC AGA GT-3') with 8 cycles of PCR amplification. Following purification with Agencourt Ampure XP beads (1:1 ratio; Beckmann Coulter), the product size distribution and the quantity were assessed on a Bioanalyzer High Sensitivity DNA Kit (Agilent). The amplified cDNA (200 ng) was fragmented for 10 min at 55 ºC using Nextera XT (Illumina) and amplified for 12 cycles with indexed Nextera PCR primers. The library was purified twice with Agencourt Ampure XP beads (0.8:1 ratio) and quantified on a Bioanalyzer using a High Sensitivity DNA Kit.

The libraries were sequenced on the HiSeq 4000 or HiSeq 2500 (Illumina) in paired-end mode. The read length for HiSeq 4000 runs was 2×76 bp, using the HiSeq 4000 SBS Kit and HiSeq 4000 PE Cluster Kit sequencing flow cell. When using the HiSeq 2500, the libraries were sequenced in paired-end mode with a read length of 2×76 bp using the TruSeq SBS Kit v4.

Primary data analysis, including image analysis, base calling, and quality scoring, was performed using the manufacturer's software: Real-Time Analysis (RTA 2.7.7) for HiSeq 4000 and RTA 1.18.66.3 for HiSeq 2500. This was followed by the generation of FASTQ sequence files.

RNA-seq data processing and analysis

Mouse RNA-seq reads were mapped against the Mus musculus reference genome (GRCm38) with STAR/2.5.3a (Dobin et al., 2013) using ENCODE parameters. Genes and isoforms were quantified with RSEM/2.3.0 (Li and Dewey, 2011) with default parameters using the gencode.M15 annotation. Likewise, rat RNA-seq reads were mapped against the Rattus norvegicus reference genome (Rnor6.0) whereas the Rnor6.0.92 annotation was used for gene and isoform quantification. The original raw and processed data are available from the Gene Expression Omnibus, accession number XXXXXXXXX
(https://www.ncbi.nlm.nih.gov/geo/query/acc.cgi?acc=XXXXXXXXX)

Differential expression analysis was performed with the R package DESeq2/1.18 (Love et al., 2014). The regularized log transformation of the counts was used for plotting. Genes with FDR<5% and |FC|>1.5 were considered significantly differentially expressed. Heatmaps were drawn with the R package 'ggplot2' using Z-score normalisation and the PCA was done with the 'prcomp' R function. Gene ontology (GO) enrichment analyses of the differentially expressed genes was performed with g:Profiler (Raudvere et al., 2019). We separately analysed the lists of upregulated or downregulated genes from each control vs treated comparison. Enrichment analyses were done also on the lists of genes similarly or differentially regulated across experiments (for instance, genes downregulated in both the streptomycin and the IDPN-4wk groups). To reduce redundancy in the lists of GO terms, the REVIGO tool (Supek et al., 2011) was used to cluster groups by semantic similarity analysis and thus generate shorter lists of cluster representatives.

In addition to GO analyses, Gene Set Enrichment Analyses (GSEA) (Subramanian et al., 2005; Mootha et al., 2003) were performed with the original expression datasets to evaluate whether the gene expression changes induced by the treatments matched any well-known biological process as defined by the Hallmark Gene Sets.

Immunohistochemical labelling.

For immunohistochemistry of the vestibular sensory epithelia, the following commercial primary antibodies were used at the indicated dilutions: mouse monoclonal anti-contactin-associated protein (CASPR1) (clone K65/35, cat.#MABN69, Millipore, RRID: AB_2083496, 1/400), mouse monoclonal anti-myosin-7A (MYO7A) (cat.# 138-1, supernatant, Developmental Studies Hybridoma Bank, RRID: AB_2282417, 1/100), rabbit anti- potassium voltage-gated channel subfamily A member 10 (KCNA10, Kv1.8)(cat.# APC-157, Alomone Labs, RRID:

AB_2341039, 1/200), rabbit anti-MYO7A (cat.# 25-6790, Proteus Biosciences, RRID: AB_10015251, 1/400), rabbit anti-oncomodulin (cat.# OMG4, Swant, RRID:AB_10000346, 1/400), rabbit anti-plasma membrane calcium transporting ATPase 2 (PMCA2, encoded by the Atp2b2 gene) (cat.# PA1-915, Invitrogen, RRID: AB_2243199, 1/400), goat anti-Delta/Notch Like EGF Repeat Containing (DNER) (cat.# AF2254, R&D Systems, RRID:AB_355202, 1/200), goat anti-Osteopontin (encoded by the Spp1 gene) (cat.# AF808, R&D Systems, RRID: AB_2194992, 1/200), and guinea pig anti-calretinin (cat.# 214104, Synaptic Systems, RRID: AB_10635160, 1/500). In addition, a rabbit anti-VSIG10L2 antibody was generated against the sequence VSXL-756:772 (DPIQESIDAPVNVTITV) using the ThermoFisher Custom Antibodies services. To reveal the primary antibodies, we used appropriate fluorochrome-conjugated donkey secondary antibodies from Invitrogen / Thermo Fisher. These included DayLight 405, and Alexa-Fluor -488, -555, and -647 fluorochromes for four-channel imaging.

Whole vestibular epithelia were immunolabelled as described previously (Greguske et al., 2019; Maroto et al., 2021, 2023). To prevent biases from batch-to-batch differences in label, equal numbers of specimens from each experimental group were processed in parallel. Briefly, the main protocol included permeation and blocking in 4% Triton-X-100 (Lysakowski et al., 2011) and 20% donkey serum in PBS for 90 min at room temperature, followed by incubation with the mixed primary antibodies in 0.1% Triton-X-100 and 1% donkey serum in PBS for 48 h at 4ºC, then by incubation with the secondary antibodies in 0.1% Triton-X-100 in PBS overnight at 4ºC. Specimens were thoroughly rinsed in PBS following each incubation and gently rocked during all incubations and rinses. To assess KCNA10 and PCMA2 immunoreactivity, the samples were first permeated at room temperature with 4% Triton-X100 for 1 h, then blocked with 1% fish gelatin (cat.# G7765, Sigma-Aldrich) for 1 h (Lysakowski et al., 2011). In this protocol, primary and secondary antibody solutions contained 0.1% Triton-X-100 and 1% fish gelatin. After immunolabelling, some batches of samples were whole-mounted in Fluoromount medium (F4680, Sigma-Aldrich), while other samples were sectioned before mounting. For sectioning, specimens were placed in 0.49% gelatin, 30% bovine serum albumin, and 20% sucrose in PBS overnight at 4ºC. The next day, the sample was oriented and included in between two fused blocks formed by solidification of the same mixture with 2 % glutaraldehyde. The block was then used to obtain 40 μm-thick sections in a Leica VT1000S vibrating microtome. This protocol has been described in detail elsewhere (Maroto et al., 2021b).

RNA scope in-situ hybridization

Vestibular epithelia were processed for simultaneous immunofluorescence and RNA-scope in-situ hybridization. We used the RNAscope Multiplex Fluorescent Reagent Kit v2 (cat. # 323100, ACD Bio-Techne) with the following probes: RNAscope® Probe - Rn-Vsig10l2- C1,PREDICTED: Rattus norvegicus V-set and immunoglobulin domain containing 10 like 2 (Vsig10l2) mRNA (cat. # 1241271-C1), RNAscope® Probe- Rn-Atf3 (cat. #414981) and Rn-Ppib-C3 - Rattus norvegicus peptidylprolyl isomerase B (Ppib) mRNA (cat. # 313921-C3) or RNAscope® Positive Control Probe - Rn-Ppib-C2 - Rattus norvegicus peptidylprolyl isomerase B (Ppib), mRNA (cat. #313921-C2) as a positive control. To label the probes, we used the fluorophores Opal 520 (cat. # FP1487001KT, Akoya Biosciences), Opal 570 (cat. # FP1488001KT), and Opal 690 (cat. # FP1497001KT). Briefly, free-floating epithelia were washed in RNAscope Wash Buffer and dehydrated with graded concentrations of ethanol. Then, samples were washed and incubated in H_2O_2 0.3% (v/v) for 10 min at RT. Sections were then hybridized in probe mixture (either Rn-Vsig10l2- C1 plus Rn-Ppib-C3 or Rn-Atf3 plus Rn-Ppib-C2 at a 50:1 concentration, as indicated by the manufacturer) inside screw microtubes for 2 h at 37ºC using a water bath. Afterwards, tissues were washed and incubated in amplification solutions Amp1, Amp2, and Amp3 for 35, 20, and 35 min, respectively, at 37ºC. For signal detection, HRP-C1 and HRP-C3/HRP-C2 solutions were added to the sections for 15 min each at 37ºC, followed by a 30 min incubation of TSA-diluted Opal 520 and Opal 570/Opal 690 at 37ºC. After washing, the sections were processed for MYO7A immunostaining with the rabbit MYO7A antibody and mounted following the protocol described above.

Confocal microscopy imaging and analysis

Vestibular epithelia were observed in a Zeiss LSM880 spectral confocal microscope. The 63x (NA=1.4) objective was used to obtain 135 x 135 μm images. Z-stacks of optical sections were obtained at 0.35 μm spanning 6 to 30 μm as required for the planned analysis. The same image acquisition settings were used for all samples from each immunolabelling batch. To measure fluorescence intensities, we used the ImageJ software (National Institute of Mental Health, Bethesda, Maryland, USA). The expression of the plasma membrane calcium-transporting ATPase (PMCA2), encoded by the *Atp2b2* gene, was evaluated in whole-mount utricles (one utricle per animal) labelled with the mouse anti-MYO7A, the anti-calretinin and the anti-PMCA2 antibodies. From each utricle 15 different areas were acquired with Z-stacks of 30 optical sections. These were then used to generate maximal intensity projections of 14-section sub-stacks for quantitative analysis. On each image, a rectangular region of interest (ROI) of 12.6 x 7.8 μm was used to assess the fluorescence intensity of the PMCA2 channel in one stereocilia bundle and the background fluorescence intensity was subtracted. From each image, at least 12 different bundles were quantified, so PMCA2-associated fluorescence for each utricle was estimated as the mean value from at least 180 (usually more than 200) individual hair bundles. To evaluate the effects of the treatments, we compared 3 control with 4 IDPN-4wk rats, and 4 control with 4 streptomycin rats.

DNER expression was quantified using whole-mount cristae labelled with the rabbit anti-MYO7A, the anti-CASPR1, the anti-calretinin and the anti-DNER antibodies. From each crista, four images were acquired, two from the central part and two from the periphery, with Z-stacks spanning up to 30 μm. For quantitative analysis, sub-stacks of 6 sections were made to select the level of the epithelium containing the supra-nuclear region of HC, and an oval ROI (diameters of 2,7 and 2,1 μm) was used to quantify fluorescence intensity from at least 60 HC per image. To evaluate the effects of the treatments, we compared 3 Control with 4 IDPN-4wk rats, and 4 Control with 4 Streptomycin rats.

KCNA10 expression was assessed in whole-mount cristae labelled with anti-osteopontin, anti-CASPR1 and anti-KCNA10 antibodies. From each crista, four images were obtained as described above for DNER. For quantitative analysis, sub-stacks of 7 sections were made to select the level of the epithelium containing the mid-lower nuclear region of HCI, to obtain circular slices of the calyceal junction adhering HCI with the afferent calyx. The ROI used for fluorescence measurement was made of three circles, 0.60 μm of diameter each, placed at the vertices of an equilateral triangle with 4.1 μm edges. From each cell, two measures were obtained, so the estimation of the fluorescence intensity was derived from 6 readings approximately evenly placed around the cell's basolateral membrane. From each image, a mean fluorescence intensity was obtained by averaging the readings of 100 HCI. To evaluate the effects of the treatments, we compared 3 Control with 3 IDPN-4wk rats, and 3 Control with 3 Streptomycin rats.

For MYO7A, osteopontin and calretinin expression analyses, 40 μm-thick sections of crista samples were imaged and fluorescence intensities determined as described in detail elsewhere (Maroto et al., 2023). Briefly, 3 μm thick Z sub-stacks were used to assess fluorescence intensity in 30 HCs per rat with a rectangular ROI. Data were normalized to control mean values of the same labelling batch to circumvent batch-to-batch differences in immunostaining. These analyses included 5 to 8 control rats and 6 to 10 IDPN-4wk rats.

Expression of the VSIG10L2 protein was evaluated in utricles (9 Control and 9 IDPN-4wk samples) labelled with the anti-VSIG10L2, the anti-osteopontin, the anti-calretinin and the monoclonal anti-MYO7A antibodies. For quantitative analysis, 27 HCs were selected from each image using a pre-defined grid. For each cell, the fluorescence intensity above background was measured in the supranuclear zone using a circular ROI (5 μm diameter).

For RNAscope analysis, Z-stacks of 50 optical sections were taken, obtained every 0.35 μm. For each epithelium, 4 images were collected in total, 2 from the centre of the epithelium and 2 from the peripheral zone. Then, the HC spanning section was selected by creating maximum intensity projections. For the analysis of ATF3

expression, the number of PPIB and ATF3 puncta was measured using the “Find maxima” tool of the ImageJ software, after thresholding for intensity. Total puncta number was averaged by individual, area, and number of HCs. To quantify VSIG and PPIB fluorescence intensity, images were thresholded to select VSIG or PPIB puncta. Then the mean grey value (ie: the fluorescence intensity) was acquired using the “Measure” function of ImageJ. This number was averaged by individual, area, and total cell count.

Statistics

Padj / FDR values were used to evaluate gene and GO enrichment. For other data, such as immunofluorescence intensity data, group comparisons were done using the Student's t-test, corrected for multiple comparisons if needed, or ANOVA test as appropriate, using the GraphPad Prism software. In all cases, the significance level was set at $p<0.05$.

2. RESULTS

2.1. SYSTEMIC AND VESTIBULAR TOXICITY

Subchronic ototoxic exposure caused a progressive loss of vestibular function with limited systemic toxicity.

In four separate experiments, we obtained RNAseq data for five different treated *vs.* control comparisons. These included 3 different models of subchronic ototoxicity (mouse/IDPN, rat/IDPN, and rat/STREP) and 3 different time points (3, 4, and 7 weeks) of the rat/IDPN model. The mouse/IDPN, rat/IDPN-4wk, and rat/STREP experiments were performed to investigate the gene expression changes associated with the behavioural and histological effects described in previous studies (Sedó-Cabezón et al., 2015; Greguske et al., 2019; Maroto et al., 2023). The rat/IDPN-3wk and rat/IDPN-7wk groups were studied as representative of earlier and later stages of the chronic ototoxicity process. As described previously (Sedó-Cabezón et al., 2015; Greguske et al., 2019; Martins-Lopes et al., 2019; Maroto et al., 2023), the exposed animals showed no overt signs of systemic toxicity besides reduced increase in body weight compared to controls in some cases (Suppl. Fig. S1). Also, as revealed in mice by vestibular dysfunction ratings (Saldaña-Ruiz et al., 2013) and in rats by the tail-lift reflex (Martins-Lopes et al., 2019; Maroto et al., 2021), the treated animals showed the expected progressive decline in vestibular function (Suppl. Fig. S2).

2.2. RNA-seq: OVERALL ANALYSIS

RNA-seq analyses identified gene sets with altered expression after subchronic ototoxic exposure.

In all four experiments, treated animals showed significant changes in gene expression with respect to control animals. In every case, principal component analysis (PCA) with the 500 most variable genes (Fig. 1A-D) resulted in one first component (PC1) that collected more than half of the variance (range 52.2 to 80.3 %) and ordered control and treated animals (n=3 in all groups). Heat maps of the 50 most significantly altered genes in each comparison between control and treated animals successfully grouped the samples according to treatment group (Fig. 1E-I). For each of these comparisons, the total number of differentially expressed genes (DEGs) and the numbers of downregulated and upregulated genes are shown in Table 1. Volcano plots, shown in Fig. 2, display these DEGs according to log2-Fold_Change and log-Padj. Comparisons across experiments revealed the presence of a significant batch effect, so the raw data could not be merged for a global analysis. Therefore, GO analyses with g:Profiler were performed separately for each treated *vs.* control comparison. Afterwards, comparisons across experiments were done by comparing both the lists of DEGs and the results of the GO analysis from each experimental model. Lists of DEGs and GO terms shared or differing across experiments or groups of experiments were obtained and evaluated as detailed throughout the text.

2.3. RNA-seq: DOWNREGULATION RESPONSES

Gene downregulation responses common to all subchronic ototoxicity models.

GO analyses of the downregulated genes identified from 59 (in rat/IDPN-3wk) to 654 (in rat/IDPN-4wk) Biological Process (BP) terms, from 22 (in rat/STREP) to 157 (in rat/IDPN-4wk) Cell Component (CC) terms, and from 26 (in rat/IDPN-3wk) to 95 (in rat/IDPN-4wk) Molecular Function (MF) terms. To obtain a focused view on the effects of the treatments we excluded from these lists terms with 1000 or more genes that are too broad. The resultant lists of enriched terms are provided with their corresponding p-values in Suppl. Tables S1. Comparison of these lists across experimental conditions revealed the presence of terms common in all comparisons. Fig. 3 shows the terms enriched in the five lists of downregulated genes, displayed according to the significance adjusted p-values in the control vs. streptomycin comparison. The most prominent group of BP terms identified by the analysis (Fig. 3A) was that of terms related to hair cell structure, development, or function. Thus, highlighted terms in all the five BP lists included among others "sensory perception of sound" (GO:0007605) and "sensory perception of mechanical stimulus" (GO:0050954), "mechanoreceptor differentiation" (GO:0042490), and "inner ear development" (GO:0048839). In addition, two other conspicuous groups of BP terms associated with the genes downregulated in all exposure conditions were identified. One was that of terms related to ion channels such as "monoatomic ion transmembrane transport" (GO:0034220). This was paralleled by a group of MF terms also identified in all five control vs. treated comparisons (Fig. 3B), that included "monoatomic cation channel activity" (GO:0005261)" and other related terms. Also enriched were several BP terms related to the synapse such as "chemical synaptic transmission" (GO:0007268), "anterograde trans-synaptic signaling"(GO:098916), "trans-synaptic signaling" (GO:0099537), and "synaptic signaling" (GO:0099536). Another prominent group of GO terms enriched among downregulated genes was that of terms related to the stereocilium. As shown in Fig. 3C, the CC terms identified in all five comparisons included among others "stereocilium bundle" (GO:0032421), "stereocilium" (GO:0032420), "cluster of actin-based cell projections" (GO:0098862), and "actin-based cell projection" (GO:0098858)".

A parallel analysis of the common gene downregulation response shared by all experimental conditions was performed by crossing the lists of gene symbols to identify the genes present in all five lists. As shown in the Venn diagram (Fig. 4A), 34 genes were identified as genes downregulated in all experimental models of ototoxicity under study. Among these genes, listed in table 2, there are trophic factors and neurotrophin receptors (*Bdnf*, *Bmp2*, *Ntrk3*), as well as proteins with known roles in terminal differentiation of HCs and stereocilium morphology (*Xirp2*, *Dner*, *Ptprq*, *Cfap126*), cell adhesion (*Cdh18*, *Adam11*), vesicular secretion (*Chgb*), stereocilium calcium pumping (*Atp2b2*) and HC potassium permeation (*Kcnab1*, *Kcna10*). Fig. 4B shows the expression heat maps of these 34 genes in the 5 control vs. treated comparisons. GO analysis of this list of 34 DEGs identified "mechanoreceptor differentiation" (GO:0042490) and "inner ear development" (GO:0048839) as the only two significantly enriched BP terms (Padj = 4.41E-03 and Padj = 6.98E-03, respectively). As shown in table 2 and discussed below, this results from the fact that 29 of these 34 genes have been previously identified to be selectively expressed by HCs within the rodent or human vestibular sensory epithelium. Thus, the data revealed the downregulation of genes with important roles in HCs mature function and terminal differentiation.

For an additional identification of genes downregulated both after either IDPN or streptomycin exposure, we compared the gene lists of the rat/STREP and rat/IDPN-4 wk experiments. The 4-week time point of IDPN exposure was selected for this additional comparison with the streptomycin data because it likely corresponded to a more similar level of toxicity than that of IDPN rats examined at earlier (3 weeks) or later (7 weeks) times of exposure. In addition to the 34 genes listed in Table 2, 108 additional genes were identified, resulting in a total of 142 genes similarly downregulated in the vestibular epithelium of streptomycin and IDPN rats (Fig. 5A). In this extended list, several additional genes encoding for important HC proteins were recognized. Thus, the list

contains the genes of the motor protein *Myo7a*, the calcium binding protein *Pvalb*, the tyrosine phosphatase *Ptprz1*, and the component of the mechanotransduction complex *Lhfpl5*, all of them known to have prominent roles in HC physiology. Accordingly, the GO analysis of this list identified "sensory perception of sound" (GO:0007605), with Padj = 5.56E-07, and "stereocilium bundle" (GO:0032421), with Padj = 2.34E-05, as the most significantly enriched BP and CC terms, respectively (Fig. 5B). An enrichment value of 1.0 in the "calcium-dependent ATPase activity" (GO:0030899) MF term revealed the decreased expression of both Atp2b2 and Atp2b3 genes, encoding the PMCA and SERCA2 proteins.

For an alternative approach to identify common downregulation responses elicited by subchronic ototoxicity exposure, we performed the threshold-free GSEAS to identify gene sets enriched in the control animals. In each experimental condition, only one or two gene sets were enriched in control compared to treated samples at FDR < 0.25, and none of them were common across models (data not shown). Therefore, no hallmark gene set was downregulated in all subchronic ototoxicity models.

Taken together, these comparisons lead to the conclusion that enduring ototoxic stress induces a decrease in the expression of HC-specific genes. Based on the histological assessment of the exposure models under study (Sedó-Cabezón et al., 2015; Greguske et al., 2019; Maroto et al., 2023) and validation data shown below, these observed decreases were not consequent to HC loss, but due to downregulation of gene expression. This downregulation response is shared by IDPN and streptomycin exposure, occurs both in rats and mice, and starts at the early stages of chronic ototoxicity in association with the initial loss of vestibular function. We also concluded (see below) that this response widens as the ototoxic stress progresses at longer times of exposure.

Compound-specific gene downregulation responses in vestibular epithelia after subchronic ototoxicity.

In addition to the identification of genes responding similarly in all exposure models, we used the datasets to identify responses differently associated with one or the other toxic compound. Using the rat/STREP and rat/IDPN-4wk datasets, we identified the genes downregulated in streptomycin rats but not in IDPN rats and those downregulated by IDPN but not by streptomycin (Fig. 5A). The 138 rat/STREP-only genes did not reveal any prominent differential response, as they were mostly genes that were not significantly downregulated in the rat/IDPN-4wk samples but that were related to GO terms downregulated also by IDPN, such as "sodium ion transmembrane transport" (GO:0035725) (Fig. 5C). The analysis of the 1620 genes unique to the rat/IDPN-4wk downregulation response identified many GO terms identified also in the rat/STREP experiment, such as "sensory perception of sound" (GO: 0007605), as explained above. However, other terms were apparently exclusive of the IDPN effect. A particularly consistent difference was that of terms related to cell adhesion, such as "cell-cell adhesion via plasma-membrane adhesion molecules" (GO:0098742), as many cadherins, protocadherins, CAMs and other adhesion factors were downregulated in the rat/IDPN-4wk but not in the rat/STREP samples (Fig. 5D). The effect of IDPN toxicity on cell adhesion was also present in the other IDPN experiments, and robust significance of many related terms, including the "cell-cell adhesion via plasma-membrane adhesion molecules", was present in the mouse/IDPN, rat/IDPN-3wk, and rat/IDPN-7wk versus control comparisons.

Downregulation responses in late stages of subchronic ototoxicity.

In the advanced stages of the subchronic IDPN toxicity, HCs alter their morphology and start extruding from the sensory epithelium to the endolymphatic cavity. Abnormal and extruding HCs accumulate in the epithelium, indicating that the process is characterized by considerable synchrony and slow progression (Seoane et al., 2001a,b; Sedó-Cabezón et al., 2015). In contrast, our previous data (Maroto et al., 2023) suggest that this form of HC demise may operate in streptomycin rats, but do so in a much more non-synchronic and fast manner, so extruding cells do not accumulate in the epithelium. To evaluate if the late damaged (i.e, extruding or pre-extruding) sensory HCs present a downregulation response different from that at earlier stages, we focused on

the genes downregulated in rat/IDPN-7wk specimens but not in rat/IDPN-3wk or rat/STREP specimens. The list included 631 genes (Fig. 6A) that, by GO analysis, associated with 95 BP terms. These terms showed a significant overlap with the terms associated with the genes similarly downregulated in all 5 models. For instance, several HC related terms, grouped by REVIGO under the term "inner ear development" (GO:0048839), were significantly altered (Fig. 6B). Therefore, more HC-specific genes were downregulated at later time points in IDPN ototoxicity than at earlier stages. Among them, there were genes such as *Atoh1* and *Pou4f3*, key transcription factors in HC differentiation, or *Cdh23* and *Ush1c*, encoding the tip-link proteins cadherin-23 and harmonin, respectively. Similarly, the cluster of enriched terms under the term "synapse organization" (GO:0050808) matched terms enriched in all five comparisons. Therefore, these observations further support the conclusion stated above that the downregulation response shared by all ototoxicity models widens at longer times of exposure. In addition, other terms derived from the list of genes downregulated after 7 weeks but not 3 weeks of IDPN exposure overlapped with those shared by all IDPN models, as the terms related to cell adhesion, indicating that additional genes from the same domain significantly reduced expression at the later stages of toxicity. Nevertheless, at least one cluster of enriched BP terms from the downregulated genes in rat/IDPN-7wk specimens but not in rat/IDPN-3wk or rat/STREP specimens represented a unique addition of the late IDPN toxicity. REVIGO selected the term "ATP synthesis coupled electron transport" (GO:0042773) to represent this cluster. Downregulated genes associated with this term were both nuclear (e.g.: *Ndufs4*) and mitochondrially-encoded (e.g.: *mt-Nd4*). So one qualitative difference between late (rat/IDPN-7wk) and early (rat/IDPN-3wk or rat/STREP) ototoxicity appears to be the downregulation of genes involved in mitochondrial respiration.

2.4. RNA-seq: UPREGULATION RESPONSES

Gene upregulation responses similarly elicited by subchronic ototoxicity in all exposure models.

GO analyses of the upregulated genes identified from 61 (in rat/IDPN-3wk) to 457 (in rat/IDPN-7wk) BP terms, from 11 (in rat/STREP) to 59 (in rat/IDPN-7wk) CC terms, and from 4 (in rat/IDPN-3wk) to 51 (in rat/IDPN-4wk) MF terms that were significantly enriched (Suppl. Tables S1). Comparison of these lists of terms across the 5 experimental evaluations identified only two CC and two MF broad terms in common (GO:0005737, "cytoplasm"; GO:0005829, "cytosol"; GO:0003824, "catalytic activity"; GO:0005515, "protein binding"). Among BPs, 23 terms were significantly enriched after all the ototoxic treatments. This list of terms, shown in Fig. 7 according to the p-adj values in the streptomycin experiment, was only moderately informative, as all of these terms were broad, including more than 1000 genes. Nevertheless, several of them related to stress responses and responses to chemicals. Comparison of the original lists of upregulated genes did not identify any gene being more expressed than in controls in all 5 comparisons (Fig 4B). However, if the mildest toxicity condition (rat/IDPN-3wk) was excluded, one single gene was found to be upregulated in the other 4 conditions, and this gene was *Atf3*. For a broader view of upregulation responses shared by IDPN and streptomycin, we compared the lists of DEGs from the rat/IDPN-4wk and rat/STREP experiments and obtained a list of 74 common upregulated genes (Fig 8A). GO analysis of this list (Fig. 8B) identified "positive regulation of transcription from RNA polymerase II promoter in response to stress" (GO:0036003) as the most significantly associated BP term, because of the presence of *Atf3*, *Atf4*, *Cebpb* and *Notch1* in the list. The list also contained five additional genes encoding components of the RNA polymerase II transcription regulatory complex (*Esf4*, *E2f6*, *Vdr*, *Taf5l*, *LOC103689931*). These results suggest that chronic ototoxic stress caused by diverse kinds of toxic compounds (IDPN and streptomycin) may trigger, in the vestibular epithelium of both rats and mice, a common stress response involving ATF3, ATF4, and Cebpb. However, this transcriptional response seems to start later than the downregulation of HC-marker genes identified above during progressive toxicity.

By GSEAS, there was a clear difference between the gene sets upregulated by IDPN and those upregulated by streptomycin, with no overlap at FDR < 0.05 (Table 3). However, streptomycin samples showed a marginal

enrichment in the p53 pathway (FDR=0.055) and MYC_Targets_V1 (FDR=0.060) gene sets, and these were significantly enriched in the IDPN groups except the IDPN/3wk group.

Compound-specific gene upregulation responses in vestibular epithelia after subchronic ototoxicity.

As previously done for the downregulated responses, we compared the rat/STREP and rat/IDPN-4wk gene lists to identify upregulation responses that may be unique to the streptomycin and IDPN toxicities. Thus, we identified a list of 293 genes that were upregulated after streptomycin but not after 4 weeks of IDPN in rats (Fig. 8A). GO analysis of this list followed by REVIGO reduction and exclusion of the broad terms (term_size > 1000) resulted in a list of 8 BP, 2 CC, and 3 MF terms (Fig. 8C). This list included "tRNA aminoacylation for protein translation" (GO:0006418) as the most significantly enriched BP term along with the CC term "aminoacyl-tRNA synthetase multienzyme complex" (GO:0017101), and the MF terms "aminoacyl-tRNA ligase activity" (GO:0004812). We noticed the significant upregulation of 9 genes encoding tRNA aminoacylation proteins like *Yars1* and *Lars1*. Other significant terms were "amino acid transmembrane transport" (BP, GO:0003333) and similar terms, due to the presence of several amino acid transporters of the Slc family, such as the high affinity cationic amino acid transporter, *Slc7a1*, and the glutamate/neutral amino acid transporter, *Slc1a4*. Therefore, subchronic streptomycin, but not IDPN, induced expression of genes involved in protein synthesis. By GSEAS, the streptomycin samples, but none of the IDPN groups, displayed a highly significant enrichment of the "unfolded protein response" hallmark gene set (Table 3).

As much as 1025 genes were upregulated in IDPN-4wk rats but not after streptomycin (Fig. 8A). After GO analysis, REVIGO downsizing and exclusion of broad terms, many BP terms related to the stress, immune, defence, and anti-viral responses were identified (Fig 8D). This resulted from the presence in the list of interferon-responsive and immune-related genes such as *Stat1*, *Stat2*, *Stat3*, *Irf7*, *Irf9*, *Oas2*, *Igtp*, *Isg15*, and many others. When we evaluated the upregulation changes in all control *vs* treated comparisons, we observed that this immune-related response was present also in all IDPN groups (mouse/IDPN, rat/IDPN-3wk, rat/IDPN-4wk, and rat/IDPN-7wk). In good agreement with these GO analyses, GSEAS identified the enrichment of several related hallmark sets of genes in common in all four IDPN vs. control comparisons but not in the streptomycin vs. control comparison (Table 3). Specifically, the gene sets "interferon-alpha response", "interferon-gamma response", "IL6-JAK-STAT3 signalling", and "allograft rejection" were significantly enriched (FDR <0.05) after IDPN but not after streptomycin.

Upregulation responses in late stages of subchronic ototoxicity.

As explained above for the downregulation responses, we searched for late ototoxicity upregulation responses by studying the list of genes upregulated in the rat/IDPN-7wk specimens but not in rat/IDPN-3wk or rat/STREP models. This list contained 518 genes (=245+273, upper right in Fig.9A). The result of the GO analysis followed by REVIGO reduction highlighted the upregulation of anti-viral response genes, revealing that the lists of upregulated interferon-stimulated genes were longer in late rather than in early IDPN exposure conditions. Thus, genes like *Stat1*, *Stat2*, *Irf7*, *Irf9*, *Igtp*, and *Isg15* were upregulated in the rat/IDPN-7wk but not in the rat/IDPN-3wk samples. Nevertheless, other genes related to anti-viral responses and interferon signalling, such as *Usp18*, *Oas1a*, *Anxa1*, *Ifitm1*, *Ifi27*, *Ifitm3*, and *Eif2ak2,* were already upregulated in the rat/IDPN-3wk sensory epithelia. For an illustration of the core response to the advanced IDPN ototoxicity, we selected the 245 genes that were upregulated in both the rat/IDPN-7wk samples and the rat/IDPN-4wk or the mouse/IDPN samples, but not in the rat/IDPN-3wk or the rat/STREP specimens. Cluster analysis of the protein-protein interactions of this list by STRING (von Mering et al., 2003; Szklarczyk et al., 2023), using an MLC inflation parameter of 2, identified the cluster of 53 proteins shown in Fig. 9B as the main result. The top BP descriptor of this cluster was "Defense response to virus" (GO:0051607; FDR = 3.10E-30) and many related terms associated to it. These included, for instance, "Response to virus" (GO:0009615; FDR =1.38E-33), "Negative regulation of viral process"

(GO:0048525; FDR = 6.28E-18), and "Response to interferon-beta" (GO:0035456; FDR = 1.12E-13), indicating that progression of the IDPN ototoxicity consistently causes broadening of an anti-viral-like expression response.

2.5. VALIDATION STUDIES

The gene downregulation response triggered by subchronic ototoxicity is associated with decreased expression of the corresponding proteins in HCs.

As explained above, all ototoxic treatments caused a reduction in the number of transcripts from 34 genes, 29 of which have been demonstrated to be selectively expressed in HCs in human or rodent vestibular epithelia. As the ototoxic treatments used cause no or only limited HC loss (Sedó-Cabezón et al., 2015; Greguske et al., 2019; Maroto et al., 2023), this suggested that vestibular HCs under sustained toxic stress downregulate the expression of genes encoding proteins that characterize their terminal differentiation and are key to their transducing roles. To further support this conclusion, we used immunofluorescent labelling and confocal microscopy to compare the expression of some of these proteins in samples from control and treated animals in the rat/IDPN-4wk and rat/STREPTO experiments. A robustly downregulated gene was *Atp2b2*, encoding the plasma membrane calcium transporting ATP-ase 2 (PMCA2). This calcium transporter is expressed in the stereocilia of auditory and vestibular HCs and extrudes calcium towards the endolymphatic cavity (Fettiplace and Nam, 2019). In the rat vestibule, we have recently described that PMCA2 is expressed by HCIs but not by HCIIs (Borrajo et al., 2024). We found that rats exposed to 20 mM of IDPN for 4 weeks had a 72% reduction (t_{5df} = 7.812, p=0.001) in fluorescence intensity of the PMCA2 label in the stereocilia bundles of the utricle (Fig. 10A, Da). Similarly, streptomycin rats (500 mg/kg/day x 6 weeks) showed an 84% reduction (t_{6df}= 11.70, p<0.001) in PMCA2 expression in utricular stereocilia (Fig. 10B, Db).

Another HC-specific downregulated gene was the *Dner* gene, encoding the Delta/Notch-like epidermal growth factor-related receptor (DNER). DNER has been shown to be necessary for proper maturation and orientation of the stereocilia bundle (Kowalik and Hudspeth, 2011). After IDPN, the crista HCs from exposed rats showed a 39 % reduction in DNER expression (t_{5df}= 2.96, p=0.031; n=3 control, 4 IDPN) (not shown). A larger effect was recorded after streptomycin, with a 63% reduction in DNER immunoreactivity in crista HCs (t_{6dg}=8.73, p<0.001) (Fig. 10C, Dc).

A third protein whose expression was assessed by immunofluorescent confocal microscopy was the potassium voltage-gated channel subfamily A member 10 (KCNA10, also known as Kv1.8), encoded by the *Kcna10* gene. Mutations in this channel cause vestibular impairment (Lee et al., 2013) and recent data have shown its strong expression in the calyceal junction area (Martin et al., 2024). In response to subchronic IDPN, the expression of KCNA10 in the calyces was significantly reduced by 50% (t(4df)=7.52, p=0.00167) (Fig. 10E, Fa). After streptomycin, the mean fluorescence value in the calyces of treated animals was 29% lower than the mean in controls (97.9 $\pm$ 14.7 vs 136.9 $\pm$ 11.5), but this difference did not attain statistical significance (t(4df)=2.091, P=0,104) (Fig 10Fb).

Beyond the list of 34 genes downregulated in all exposed groups, we also aimed to evaluate other HC-specific genes that were downregulated in several exposure conditions and for which reliable antibodies were available. Thus, we assessed the fluorescence intensity associated with anti-osteopontin, anti-calretinin, and anti-MYO7A immunolabelling in rat/IDPN-4wk samples because their encoding genes were down-regulated in this group (*Spp1* [log2-Fold_Change=-1.84; Padj=2.94E-14]; *Calb2* [log2-Fold_Change=-2.17; Padj=9.75E-22]; *Myo7a* [log2-Fold_Change=-0.64; Padj=9.67E-09], respectively). As shown in Fig. 10 G-J, a decrease in immunolabel was recorded with anti-osteopontin (HCI, t(16 d.f.)= 7.65, p=0.000) and anti-calretinin (HCII, t(9d.f.)=6.7, p=0.000) but not with anti-MYO7A (all HCs, t(15 d.f.)=0.627, p=0.27) antibodies. Differing from this MYO7A result, we had previously recorded a significant decrease in MYO7A expression in streptomycin compared to control rats (Maroto et al., 2023).

Overall, the immunohistochemical data confirmed that the decreases in expression of HC-specific genes revealed by the RNA-seq data associate with decreases in protein expression and are not an artefact resulting from HC loss.

***Vsig10l2* is a new HC-specific gene strongly downregulated during HC stress.**

Among the 34 genes downregulated in all 5 groups of rats exposed to ototoxicity, a prominent position was occupied by the *Vsig10l2* gene (previously identified as *Gm1113* in the mouse and *AC132671* in the rat). Compared to its expression in their respective controls, this gene was the most significantly downregulated in the rat/STREPTO, rat/IDPN-3wk and rat/IDPN-7wk groups, and was ranked position 14 in mouse/IDPN and 75 in rat/IDPN-4wk groups. By combined RNAscope *in situ* hybridisation and MYO7A immunohistochemistry we noticed that many, but not all, HCs expressed *Vsig10l2* (Fig 11A). By measuring fluorescence intensity, we corroborated that these HCs had a large decrease in *Vsig10l2* mRNA expression in the rat/IDPN-4wk samples (Fig. 11 A,C). While the number of HCs per image was not affected by IDPN exposure neither in the centre of the crista (control and IDPN mean values = 73.4+2.5 vs 77.8+3.9, respectively; t=0.75, 6 df, p=0.38) nor in its periphery (97.6+6.2 vs. 97.3+2.7; t=0.06, 6 df, p=0.96), the fluorescence intensity per HC of the *Vsig10l2* mRNA was decreased in both areas (Fig 11C, centre: t=4.99, 6 df, p=0.002; periphery: t=6.91, 6 df, p=0.0004). In contrast, the signal associated with the control gene *Ppib* mRNA was not changed by IDPN (Fig 11C, centre and periphery p values were 0.53 and 0.72, N.S.). We also evaluated the immunofluorescence associated with an anti-VSIG10L2 rabbit antiserum, in co-labelling experiments with anti-osteopontin and anti-calretinin antibodies. The results showed anti-VSIG10L2 immunoreactivity in HCIs but not in HCIIs (Fig 11B), and a strong decrease of this label in samples from IDPN-4wk rats. (Fig 11 B,D).

HCs under chronic stress increase ATF3 expression.

The RNAseq data identified *Atf3* as the first stress gene upregulated by both IDPN and streptomycin in the vestibular sensory epithelium of rats and mice, so we aimed at ascertaining that this corresponded to a HC response. To this end, *Atf3* and control gene *Ppib* RNAscope puncta were quantified in MYO7A-positive cells (Fig 12). The quantitative data (Fig12B) demonstrated than a specific increase in *Atf3* mRNA expression occurs in rat HCs after exposure to IDPN-4wk. Adjusted t-values of the puncta density per HC were centre: t=3.194, 12 df, p=0.0154; periphery: t= 2.738, 12 df, p=0.0357.

DISCUSSION

The molecular mechanisms involved in HC damage from ototoxic exposure have been the subject of extensive research efforts (reviewed by Kros and Steyger, 2019). However, most of these efforts have focused on the identification of events leading to fast HC degeneration by high-dose exposure or using *in vitro* models. In the present study, we aimed at identifying the main gene expression changes associated with the physiopathological response of the vestibular epithelium to sustained ototoxic stress. We hypothesize that this response is more relevant to human health than those revealed through *in vitro* or acute high-dose exposure models. To better target the most fundamental responses, we studied different species and ototoxic compounds. However, this resulted in a batch effect that impeded the direct merge of the raw data for comparison. This came as no surprise, because the four RNA-seq experiments presented here, encompassing five control *vs.* treated comparisons, were carried out over several years in parallel with the experiments that characterized the mouse/IDPN, rat/IDPN and rat/STREP models published elsewhere (Sedó-Cabezón et al., 2015; Greguske et al., 2019; Martins-Lopes et al., 2019; Maroto et al., 2023) and were performed by different experimenters. Notwithstanding, comparisons of the lists of DEGs and GO terms across experiments provided meaningful insights into the response of the vestibular epithelium to chronic ototoxic stress, as summarized in Fig. 13. These comparisons revealed common gene expression changes that open new paths in our understanding of the

mechanisms leading to HC loss. Besides its interest regarding HC biology, this knowledge may guide the identification of targets for effective treatments to prevent or block damage progression.

The individual analyses of the transcriptomic data (Fig. 1 and 2) demonstrated that each of the exposure conditions caused a gene expression response, as in each experiment control and treated animals were grouped by their gene expression profiles. Comparison across experiments revealed that the earliest and most consistent response is a robust downregulation of HC-specific genes, present already at the mildest exposure condition (rat/IDPN-3wk) and broadening in longer exposures. As we used bulk mRNA analysis from whole tissue, loss of HC-specific mRNAs could be consequent to HC loss. However, data in the present (Fig. 10-12) and previous (Sedó-Cabezón et al., 2015; Greguske et al., 2019; Maroto et al., 2023) studies demonstrate that the recorded decreases in mRNA counts of HC genes were not due to HC loss, but were associated with decreased expression of the genes and of the corresponding proteins. In previous behavioural and histological studies of chronic ototoxicity, (Sedó-Cabezón et al., 2015; Greguske et al., 2019; Maroto et al., 2023) we concluded that a reversible suspension of HC function (transduction and synaptic transmission) precedes overt signs of HC damage such as fusion of stereocilia. The transcriptomic response recorded in the vestibular ganglion (Greguske et al., 2023) also supports this HC silencing phenomenon. The present data indicate that this early step in chronic ototoxicity includes a downregulation of selective HC genes, including stereocilium, synaptic, and ion channel genes. This change in the gene expression phenotype of the HCs under stress is congruent with the subsequent loss of specific HC features shown by the cells when progressing towards extrusion. It is worth noting that this change may add difficulty to the interpretation of expression data from damaged vestibular epithelia in search for evidence of atypical HCs potentially denoting HC regeneration (Taylor et al. 2018; Wang et al., 2024).

Of the 34 genes downregulated in all exposure conditions, 29 have been previously identified to be selectively expressed by HCs within the rodent or human vestibular sensory epithelium (Scheffer et al., 2015; Sadler et al., 2020; Wu et al., 2013; Burns et al., 2015; Wang et al., 2024). The other 5 genes have not been identified neither as HC nor as supporting cell specific genes, but one of them has a role in stereocilium development (*Cfap126*; Gegg et al, 2014) and another one causes hearing impairment when mutated (*Fam107b*; White et al., 2013), so it is likely that these are also HC genes. Likewise, it is tempting to speculate that the 3 other unascribed genes (*Ntrk3*, *Osbpl11*, *Rasal2*) are also expressed by HCs rather than SCs.

More HC-specific genes were identified in the list of 142 genes downregulated in both the rat/STREP and rat/IDPN-4-wk groups. By GO analysis, these genes mostly associated with HC-specific BP (e.g., sensory perception of sound) and CC (e.g., stereocilium bundle) terms (Fig. 5B), reinforcing the conclusion that downregulation of HC-specific genes is the main response of HCs to chronic ototoxic stress. We hypothesize that the list also contains genes with significant roles in HC differentiation or mature function that have not been studied yet. It is also worth noting that several of the more significantly downregulated genes have been identified as selectively expressed in HCI *vs* HCII by immunohistochemistry in rodents (PMCA2, product of the *Atp2b2* gene, Borrajo et al., 2024) or by transcriptomic analysis in humans (*Adam11*, *Atp2b2*, *Bdnf*, *Bmp2*, *Chgb*, *Fbxw7*, *Kcnab1*, *Ocm*/*Ocm2*, *Vsig10l2*, Wang et al., 2024). Although genes expressed by both HCIs and HCIIs, such as *Dner,* were also identified, the data likely reflects the greater susceptibility of HCIs with respect to HCIIs to ototoxicity caused by either IDPN (Maroto et al., 2021a) or streptomycin (Maroto et al., 2023). Another aspect worth discussing is the downregulation of the *Atp2b2* and *Atp2b3* genes, encoding the calcium-dependent ATP-ases, PMCA2 and SERC2. Besides the essential role of PMCA2 in stereocilium mechanotransducer function (Fettiplace and Nam, 2019), reduced activity of these calcium pumps may cause cytosolic calcium overload triggering cell demise (Fettiplace and Nam, 2019; VanHouten et al., 2010).

Among the genes more robustly downregulated by chronic ototoxicity we identified a gene, *Vsig10l2* (V-set and immunoglobulin domain containing 10 like 2), for which there was virtually no information. Automatic

annotation in UniProt predicts a signal peptide and Alpha-fold (Jumper et al., 2021; Varadi et al., 2024) predicts a cell-adhesion protein with five immunoglobulin, one fibronectin-type III, and one transmembrane domains. The RNA-scope and immunohistochemical data shown in Fig. 11 demonstrated that this gene is selectively expressed in HCIs and strongly downregulated following ototoxic stress. While the role of this gene in HCI function remains to be elucidated, its interest as a marker of HCI stress becomes obvious. Recent studies in human vestibular epithelia have also identified the *Vsig10l2* gene as a specific HCI marker (Wang et al., 2024).

The downregulation of HC-specific genes preceded a second response identified in both rats and mice and after either streptomycin or IDPN exposure: the increased expression of *Atf3*, a well-known hub mediator of cell stress responses (Heinrich et al., 2024) and related genes. Surprisingly, only recently has ATF3 been identified, using HEI-OC1 cells, as a candidate player in aminoglycoside (Zhang et al., 2022) and cisplatin (Lee et al., 2022) ototoxicity. More recently, increased *Atf3* expression has been recorded 1h after noise exposure in cochlear tissue and in HEI-OC1 cells after stress triggered by tert-butyl hydroperoxide exposure (Liang et al., 2024). The work by Zhang et al. (2022) demonstrated increased *Atf3* mRNA and protein levels in the cells exposed to neomycin and presented evidence that this increase could impair mitophagy through transcriptional inhibition of the mitophagy regulator *Pink1*. However, we recorded no changes in *Pink1* expression in the present experiments. As a stress mediator, *Atf3* promotes either survival/repair or cell-demise responses (Hunt et al., 2012), so further research is needed to determine the potential role of this transcription factor in driving the reversible detachment and synaptic uncoupling shown by HCs at the early stages of chronic toxicity or in their subsequent determination to demise by extrusion.

Besides the common responses, our data also revealed some responses unique to each ototoxicity model. When discussing these results, we must keep in mind that the present work does not include experiments determining whether these effects were associated with the HCs or other types of cells in the epithelium used for RNA extraction. Beyond this cautionary note, one first conclusion is that the existence of these model-specific responses reinforce the value of the responses previously identified in both models as fundamental responses of the HC to different kinds of toxic stress. By contrast, the responses unique to each model may offer clues to mechanisms of toxicity that are compound-specific. This may be the case for the upregulation of the unfolded protein response and tRNA aminoacylation BPs after streptomycin, which may perhaps be related to the effect of aminoglycosides on ribosomal translation (O'Sullivan et al., 2017). Similarly, the downregulation of mitochondrial ATP synthesis might point to a nitrile-specific effect. However, a number of facts suggest that two robust and time-increasing responses found after IDPN and not observed in the streptomycin model, may be of broad, rather than IDPN-specific, significance. First, the downregulation of cell adhesion genes fits well with the loss of cell adhesion contributing towards HC extrusion, a phenomenon observed not only after chronic IDPN (Seoane et al., 2021a,b; Sedó-Cabezón et al., 2015; Greguske et al., 2019), but also after chronic streptomycin (Maroto et al., 2023). In these studies, a marked contrast was noticed between the slow and highly synchronous process of HC extrusion triggered by IDPN and the likely fast and asynchronous extrusion of HCs after streptomycin (Maroto et al., 2023). It is thus possible that streptomycin also triggers downregulation of cell adhesion genes but that not enough affected cells are simultaneously present in the epithelium for the detection of this effect in bulk analysis. The second important dissimilar response is the upregulation of interferon responsive genes in an anti-viral-like or inflammatory-like response. Increased expression of interferon-responsible genes can occur following toxic stress, through nitrosylation of ISG15 and subsequent activation of the ISGylation process (Zhang and Zhang, 2011). Alternatively, such a response can also be triggered by oxidative stress-induced phosphorylation of STAT1, and in fact, this has been reported to occur in HCs following cisplatin or aminoglycoside exposure (Schmitt et al., 2009; Levano and Bodmer, 2015; Kaur et al., 2016; Borse et al., 2017). Again, the bulk epithelium approach used here, selected to circumvent the confounding effects of stress caused by the cell isolation protocols, may have lacked sensitivity to detect this response in the streptomycin samples. Although still speculative, the hypothesis that decreased expression of cell adhesion genes and increased expression of interferon-regulated genes are responses of broad significance

in chronic vestibular dysfunction is supported by a recent work by Kulasooriya et al. (BioRxiv). Using single-cell transcriptomics to compare young and old vestibular HCs in the mouse, these authors identified in the old samples, among other responses, 1) downregulation of hair bundle, mechanotransduction, synapse, and HC-specific genes; 2) downregulation of cell-cell adhesion genes; and 3) increase in pro-inflammatory genes indicating potential maintenance of a prolonged low-grade inflammatory state. Another study (Paplou et al., 2023) has also reported decreased expression of cell adhesion genes and increased expression of inflammation-related genes, even though the use of the entire (bone-encapsulated) vestibule likely reduced the sensitivity of the study. Therefore, these may indeed be common responses of HCs to chronic stress. In support of this conclusion, we have recorded cellular evidence of decreased HC adhesion in human vestibular epithelia affected by a neighbouring tumour likely causing inflammatory stress (Maroto et al., 2023).

In summary, the present study compared the RNA-seq results from four experiments involving five control *vs.* chronic ototoxicity conditions. The data obtained identified that a marked downregulation in HC-specific genes occurs as the earliest response to the chronic stress. Among well-known stress responses, *Atf3* upregulation was recorded in both rats and mice and after both IDPN and streptomycin exposure. In contrast, other prominent responses were identified after one compound-specific exposure, notably the unfolded protein response identified in streptomycin exposed rats, and the down regulation of cell adhesion and upregulation of an anti-viral-like response identified in rats and mice after IDPN exposure. These require further research to establish their link to particular mechanisms of ototoxicity or to reveal their broader role.

BIBLIOGRAPHY

Borse V, Al Aameri RFH, Sheehan K, Sheth S, Kaur T, Mukherjea D, Tupal S, Lowy M, Ghosh S, Dhukhwa A, Bhatta P, Rybak LP, Ramkumar V (2017) Epigallocatechin-3-gallate, a prototypic chemopreventative agent for protection against cisplatin-based ototoxicity. Cell Death Dis 8(7): e2921.

Boyes WK, Pouyatos B, Llorens J (2020) Sensory function. In: An introduction to interdisciplinary toxicology: from molecules to man. Edited by Pope C.N. and Liu J., pp 245-260. Academic Press - Elsevier.

Burns JC, Kelly MC, Hoa M, Morell RJ, Kelley MW (2015) Single-cell RNA-Seq resolves cellular complexity in sensory organs from the neonatal inner ear. Nature Commun 6: 8557.

Dobin A, Davis CA, Schlesinger F, Drenkow J, Zaleski C, Jha S, Batut P, Chaisson M, Gingeras TR (2013) STAR: ultrafast universal RNA-seq aligner. Bioinformatics. 29: 15-21.

Eatock RA, Songer JE (2011) Vestibular hair cells and afferents: two channels for head motion signals. Ann Rev Neurosci 34: 501–534.

Fettiplace R, Nam JH (2019) Tonotopy in calcium homeostasis and vulnerability of cochlear hair cells. Hear Res 376: 11–21.

Furness DN (2015) Molecular basis of hair cell loss. Cell Tissue Res 361: 387-399.

Gegg M, Böttcher A, Burtscher I, Hasenoeder S, Van Campenhout C, Aichler M, Walch A, Grant SG, Lickert H (2014) Flattop regulates basal body docking and positioning in mono- and multiciliated cells. Elife 3: e03842.

Granados O, Meza G (2005) Streptidine, a metabolic derivative produced after administration of streptomycin in vivo, is vestibulotoxic in rats. Histol Histopathol 20: 357-364.

Greene M, Lai Y, Pajcini K, Bailis W, Pear WS, Lancaster E (2016) Delta/Notch-Like EGF-Related Receptor (DNER) is not a notch ligand. PloS One 11(9): e0161157.

Greguske EA, Carreres-Pons M, Cutillas B, Boadas-Vaello P, Llorens J (2019) Calyx junction dismantlement and synaptic uncoupling precede hair cell extrusion in the vestibular sensory epithelium during sub-chronic 3,3'-iminodipropionitrile ototoxicity in the mouse. Arch Toxicol 93: 417-434.

Heinrich R, Aronheim A, Cheng YC, Perlman I (2024) ATF3: a crucial stress-responsive gene of glia and neurons in CNS. Front Mol Neurosci 17: 1484487.

Hirose K, Westrum LE, Stone JS, Zirpel L, Rubel EW (1999) Dynamic studies of ototoxicity in mature avian auditory epithelium. Ann NY Acad Sci 884: 389-409.

Hoffman LF, Choy KR, Sultemeier DR, Simmons DD (2018) Oncomodulin expression reveals new insights into the cellular organization of the murine utricle striola. J Assoc Res Otolaryngol 19: 33-51.

Hunt D, Raivich G, Anderson PN (2012) Activating transcription factor 3 and the nervous system. Front Mol Neurosci 5:7.

Jumper J, Evans R, Pritzel A, Green T, Figurnov M, Ronneberger O, Tunyasuvunakool K, Bates R, Žídek A, Potapenko A, Bridgland A, Meyer C, Kohl SAA, Ballard AJ, Cowie A, Romera-Paredes B, Nikolov S, Jain R, Adler J, Back T, Petersen S, Reiman D, Clancy E, Zielinski M, Steinegger M, Pacholska M, Berghammer T, Bodenstein S, Silver D, Vinyals O, Senior AW, Kavukcuoglu K, Kohli P, Hassabis D (2021) Highly accurate protein structure prediction with AlphaFold. Nature 596: 583-589.

Kaur T, Borse V, Sheth S, Sheehan K, Ghosh S, Tupal S, Jajoo S, Mukherjea D, Rybak LP, Ramkumar V (2016) Adenosine A1 receptor protects against cisplatin ototoxicity by suppressing the NOX3/STAT1 inflammatory pathway in the cochlea. J Neurosci 36: 3962-3977.

Kowalik L, Hudspeth AJ (2011) A search for factors specifying tonotopy implicates DNER in hair-cell development in the chick's cochlea. Dev Biol 354: 221-231.

Kros CJ, Steyger PS (2019) Aminoglycoside- and cisplatin-induced ototoxicity: mechanisms and otoprotective strategies. Cold Spring Harb Perspect Med 9: a033548.

Kulasooriya S, Liu H, Vijayakumar S, Bloom C, Tu S, Borgmeier BJ, Zhou M, Tao L, Kachar B, He DZ (2025) Single-cell transcriptomics unravel stereocilia degeneration as a key contributor to age-related vestibular dysfunction in mice and humans. bioRxiv [Preprint]. 6:2025.02.02.636113. doi: 10.1101/2025.02.02.636113.

Lee SI, Conrad T, Jones SM, Lagziel A, Starost MF, Belyantseva IA, Friedman TB, Morell RJ (2013). A null mutation of mouse Kcna10 causes significant vestibular and mild hearing dysfunction. Hear Res 300: 1–9.

Lee S, Choi S, Park SH, Im GJ, Chang J (2022) Transcriptomic analysis of the effect of metformin against cisplatin-induced ototoxicity: a potential mechanism of metformin-mediated inhibition of thioredoxin-interacting protein (TXNIP) gene expression. Curr Issues Mol Biol 45: 286–310.

Levano S, Bodmer D (2015) Loss of STAT1 protects hair cells from ototoxicity through modulation of STAT3, c-Jun, Akt, and autophagy factors. Cell Death Dis 6: e2019.

Li B, Dewey CN (2011) RSEM: accurate transcript quantification from RNA-Seq data with or without a reference genome. BMC Bioinformatics 12: 323.

Li L, Nevill G, Forge A (1995) Two modes of hair cell loss from the vestibular sensory epithelia of the guinea pig inner ear. J Comp Neurol 355: 405-417.

Liang R, Wang W, Gao W, Li S, Lu P, Chen J, Ding X, Ma P, Yuan H, Lun Y, Guo J, Wang Z, Mei H, Lu L (2024) Calcitriol alleviates noise-induced hearing loss by regulating the ATF3/DUSP1 signalling pathway. Ecotoxicol Environ Saf 284: 116906.

Llorens J, Rodríguez-Farré E (1997) Comparison of behavioral, vestibular, and axonal effects of subchronic IDPN in the rat. Neurotoxicol Teratol 19: 117-127.

Love MI, Huber W, Anders S (2014) Moderated estimation of fold change and dispersion for RNA-seq data with DESeq2. Genome Biol 15: 550.

Lysakowski A, Gaboyard-Niay S, Calin-Jageman I, Chatlani S, Price SD, Eatock RA (2011) Molecular microdomains in a sensory terminal, the vestibular calyx ending. J Neurosci 31: 10101–10114.

Maroto, A. F., Barrallo-Gimeno, A. and Llorens, J. (2021a). Relationship between vestibular hair cell loss and deficits in two anti-gravity reflexes in the rat. Hear. Res. 410, 108336. doi: 10.1016/j.heares.2021.108336

Maroto, A.F., Greguske, E.A., Barrallo-Gimeno, A. and Llorens, J. (2021b) Evaluation of cellular and molecular pathology in the rodent vestibular sensory epithelia by immunofluorescent staining and confocal microscopy. In: Experimental Neurotoxicology Methods, Neuromethods, vol. 172, Llorens, J. and Barenys. M., Editors. Springer US, pp 35-50.

Maroto, A.F., Greguske, E.A., Deulofeu, M., Boadas-Vaello, P. and Llorens, J. (2021c) Behavioral assessment of vestibular dysfunction in rats. In: Experimental Neurotoxicology Methods, Neuromethods, vol. 172, Llorens, J. and Barenys. M., Editors. Springer US, pp 199-215.

Maroto AF, Borrajo M, Prades S, Callejo À, Amilibia E, Pérez-Grau M, Roca-Ribas F, Castellanos E, Barrallo-Gimeno A, Llorens J. The vestibular calyceal junction is dismantled following subchronic streptomycin in rats and sensory epithelium stress in humans. Arch Toxicol. 2023 Jul;97(7):1943-1961. doi: 10.1007/s00204-023-03518-z. Epub 2023 May 17. PMID: 37195449; PMCID: PMC10256663.

Martin HR, Lysakowski A, Eatock RA. The potassium channel subunit KV1.8 (Kcna10) is essential for the distinctive outwardly rectifying conductances of type I and II vestibular hair cells. Elife. 2024 Dec 3;13:RP94342. doi: 10.7554/eLife.94342. PMID: 39625061; PMCID: PMC11614384.

Martins-Lopes, V., Bellmunt, A., Greguske, E.A., Maroto, A.F., Boadas-Vaello, P. and Llorens, J. (2019) Quantitative assessment of anti-gravity reflexes to evaluate vestibular dysfunction in rats. J. Assoc. Res. Otolaryngol. 20, 553-563.

McInturff S, Burns JC, Kelley MW (2018) Characterization of spatial and temporal development of Type I and Type II hair cells in the mouse utricle using new cell-type-specific markers. Biol Open 7: bio038083. doi: 10.1242/bio.038083

Mootha VK, Lindgren CM, Eriksson KF, Subramanian A, Sihag S, Lehar J, Puigserver P, Carlsson E, Ridderstråle M, Laurila E, Houstis N, Daly MJ, Patterson N, Mesirov JP, Golub TR, Tamayo P, Spiegelman B, Lander ES, Hirschhorn JN, Altshuler D, … Groop LC (2003) PGC-1alpha-responsive genes involved in oxidative phosphorylation are coordinately downregulated in human diabetes. Nat Gen, 34: 267–273.

Nakagawa T, Yamane H, Shibata S, Nakai Y (1997) Gentamicin ototoxicity induced apoptosis of the vestibular hair cells of guinea pigs. Eur Arch Otorhinolaryngol 254: 9-14.

O'Sullivan ME, Perez A, Lin R, Sajjadi A, Ricci AJ, Cheng AG (2017) Towards the prevention of aminoglycoside-related hearing loss. Front Cell Neurosci 11: 325.

Paplou VG, Schubert NMA, van Tuinen M, Vijayakumar S, Pyott SJ (2023) Functional, morphological and molecular changes reveal the mechanisms associated with age-related vestibular loss. Biomolecules 13:1429.

Picelli S, Faridani OR, Björklund AK, Winberg G, Sagasser S, Sandberg R (2014) Full-length RNA-seq from single cells using Smart-seq2. Nat Protoc, 9: 171–181.

Raudvere U, Kolberg L, Kuzmin I, Arak T, Adler P, Peterson H, Vilo, J (2019) g:Profiler: a web server for functional enrichment analysis and conversions of gene lists (2019 update). Nucleic Acids Res 47, W1: W191-W198.

Rubel EW, Furrer SA, Stone JS (2013) A brief history of hair cell regeneration research and speculations on the future. Hear Res 297: 42-51.

Sadler, E., Ryals, M. M., May, L. A., Martin, D., Welsh, N., Boger, E. T., Morell, R. J., Hertzano, R., & Cunningham, L. L. (2020). Cell-specific transcriptional responses to heat shock in the mouse utricle epithelium. Front. Cell. Neurosci., 14, 123. https://doi.org/10.3389/fncel.2020.00123

Saldaña-Ruíz S, Boadas-Vaello P, Sedó-Cabezón L, Llorens J (2013) Reduced systemic toxicity and preserved vestibular toxicity following co-treatment with nitriles and CYP2E1 inhibitors: a mouse model for hair cell loss. J Assoc Res Otolaryngol 14: 661-671.

Scheffer DI, Shen J, Corey DP, Chen ZY (2015) Gene expression by mouse inner ear hair cells during development. J Neurosci 35: 6366–6380.

Schenberg L, Palou A, Simon F, Bonnard T, Barton CE, Fricker D, Tagliabue M, Llorens J, Beraneck M (2023) Multisensory gaze stabilization in response to subchronic alteration of vestibular type I hair cells. Elife 12:RP88819.

Schmitt NC, Rubel EW, Nathanson NM (2009) Cisplatin-induced hair cell death requires STAT1 and is attenuated by epigallocatechin gallate. J Neurosci 29:3843-3851.

Sedó-Cabezón L, Jedynak P, Boadas-Vaello P, Llorens J (2015) Transient alteration of the vestibular calyceal junction and synapse in response to chronic ototoxic insult in rats. Dis Model Mech 8: 1323-1337.

Seoane A, Demêmes D, Llorens J (2001a) Relationship between insult intensity and mode of hair cell loss in the vestibular system of rats exposed to 3,3'-iminodipropionitrile. J Comp Neurol 439: 385-399.

Seoane A, Demêmes D, Llorens J (2001b) Pathology of the rat vestibular sensory epithelia during subchronic 3,3'-iminodipropionitrile exposure: hair cells may not be the primary target of toxicity. Acta Neuropathol 102: 339-348.

Soler-Martín C, Díez-Padrisa N, Boadas-Vaello P, Llorens J (2007) Behavioral disturbances and hair cell loss in the inner ear following nitrile exposure in mice, guinea pigs and frogs. Toxicol Sci 96: 123-132.

Subramanian A, Tamayo P, Mootha VK, Mukherjee S, Ebert BL, Gillette MA, Paulovich A, Pomeroy, SL, Golub TR, Lander ES, Mesirov JP (2005) Gene set enrichment analysis: a knowledge-based approach for interpreting genome-wide expression profiles. Proc Natl Acad Sci USA 102: 15545–15550.

Supek F, Bošnjak M, Škunca N, Šmuc T (2011) REVIGO summarizes and visualizes long lists of Gene Ontology terms. PLoS ONE 6: e21800.

Szklarczyk D, Kirsch R, Koutrouli M, Nastou K, Mehryary F, Hachilif R, Annika GL, Fang T, Doncheva NT, Pyysalo S, Bork P‡, Jensen LJ‡, von Mering C‡ (2023) The STRING database in 2023: protein–protein association networks and functional enrichment analyses for any sequenced genome of interest. Nucleic Acids Res 51: D638-646.

Taylor RR, Filia A, Paredes U, Asai Y, Holt JR, Lovett M, Forge A (2018) Regenerating hair cells in vestibular sensory epithelia from humans. Elife 7: e34817.

VanHouten J, Sullivan C, Bazinet C, Ryoo T, Camp R, Rimm DL, Chung G, Wysolmerski J (2010) PMCA2 regulates apoptosis during mammary gland involution and predicts outcome in breast cancer. Proc Natl Acad Sci U S A 107: 11405-11410.

Varadi M, Bertoni D, Magana P, Paramval U, Pidruchna I, Radhakrishnan M, Tsenkov M, Nair S, Mirdita M, Yeo J, Kovalevskiy O, Tunyasuvunakool K, Laydon A, Žídek A, Tomlinson H, Hariharan D, Abrahamson J, Green T, Jumper J, Birney E, Steinegger M, Hassabis D, Velankar S (2024) AlphaFold Protein Structure Database in 2024: providing structure coverage for over 214 million protein sequences. Nucleic Acids Res 52: D368-D375.

Vitale I, Pietrocola F, Guilbaud E, Aaronson SA, Abrams JM, Adam D, Agostini M, Agostinis P, Alnemri ES, Altucci L, Amelio I, Andrews DW, Aqeilan RI, Arama E, Baehrecke EH, Balachandran S, Bano D, Barlev NA, Bartek J, Bazan NG, … Galluzzi L (2023). Apoptotic cell death in disease-Current understanding of the NCCD 2023. Cell Death Diff 30: 1097–1154.

Völkner M, Wagner F, Steinheuer LM, Carido M, Kurth T, Yazbeck A, Schor J, Wieneke S, Ebner LJA, Del Toro Runzer C, Taborsky D, Zoschke K, Vogt M, Canzler S, Hermann A, Khattak S, Hackermüller J, Karl MO (2022) HBEGF-TNF induce a complex outer retinal pathology with photoreceptor cell extrusion in human organoids. Nat Commun 13: 6183.

von Mering C, Huynen M, Jaeggi D, Schmidt S, Bork P‡, Snel B (2003) STRING: a database of predicted functional associations between proteins. Nucleic Acids Res 31:258-261.

Wang T, Ling AH, Billings SE, Hosseini DK, Vaisbuch Y, Kim GS, Atkinson PJ, Sayyid ZN, Aaron KA, Wagh D, Pham N, Scheibinger M, Zhou R, Ishiyama A, Moore LS, Maria PS, Blevins NH, Jackler RK, Alyono JC, Kveton J, Navaratnam D, Heller S, Lopez IA, Grillet N, Jan TA, Cheng AG (2024) Single-cell transcriptomic atlas reveals increased regeneration in diseased human inner ear balance organs. Nat Commun 15: 4833.

White JK, Gerdin AK, Karp NA, Ryder E, Buljan M, Bussell JN, Salisbury J, Clare S, Ingham NJ, Podrini C, Houghton R, Estabel J, Bottomley JR, Melvin DG, Sunter D, Adams NC; Sanger Institute Mouse Genetics Project; Tannahill D, Logan DW, Macarthur DG, Flint J, Mahajan VB, Tsang SH, Smyth I, Watt FM, Skarnes WC, Dougan G, Adams DJ, Ramirez-Solis R, Bradley A, Steel KP (2013) Genome-wide generation and systematic phenotyping of knockout mice reveals new roles for many genes. Cell 154: 452-464.

Wu L, Sagong B, Choi JY, Kim UK, Bok J (2013). A systematic survey of carbonic anhydrase mRNA expression during mammalian inner ear development. Dev Dyn 242: 269–280.

Zhang Y, Fang Q, Wang H, Qi J, Sun S, Liao M, Wu Y, Hu Y, Jiang P, Cheng C, Qian X, Tang M, Cao W, Xiang S, Zhang C, Yang J, Gao X, Ying Z, Chai R (2023) Increased mitophagy protects cochlear hair cells from aminoglycoside-induced damage. Autophagy 19: 75-91.

Zhang D, Zhang DE (2011) Interferon-stimulated gene 15 and the protein ISGylation system. J Interferon Cytokine Res 31: 119-130.

Table 1. Number of Differentially Expressed Genes between control and treated animals (n=3/group)

Species	**Mouse**	**Rat**	**Rat**		**Rat**
Ototoxic compound	**IDPN**	**IDPN**	**IDPN**		**Streptomycin**
			Same controls		
Control vs.:	**30 mM in d.w., 8 wk**	**20 mM in d.w., 4 wk**	**20 mM in d.w., 3 wk**	**20 mM in d.w., 7 wk**	**500 mg/kg per·day, 6 wk**
DEGs	1134	2682	1183	1885	647
Downregulated	695	1763	699	1084	280
Upregulated	439	1099	484	801	367

Table 2. Genes down-regulated in all models

Gene symbol	Name	HC vs SC Selectivity
Ablim2	Actin binding LIM protein family, member 2	Yes
Adam11	ADAM metallopeptidase domain 11	Yes
Ap3b2	Adaptor related protein complex 3 subunit beta 2	Yes
Atp2b2	ATPase plasma membrane Ca2+ transporting	Yes
Bdnf	Brain-derived neurotrophic factor	Yes
Bmp2	Bone morphogenetic protein 2	Yes
Capsl	Calcyphosine-like	Yes
Car12	Carbonic anhydrase 12	Yes
Ccdc33	Coiled-coil domain containing 33	Yes
Cdh18	Cadherin 18	Yes
Cfap126	Cilia and flagella associated protein 126	-
Chgb	Chromogranin B	Yes
Dner	Delta/notch-like EGF repeat containing	Yes
Faim2	Protein lifeguard 2-like	Yes
Fam107b	Family with sequence similarity 107, member B	-
Fbxw7	F-box and WD repeat domain containing 7	Yes
Hs3st2	Heparan sulfate-glucosamine 3-sulfotransferase 2	Yes
Hsd17b7	Hydroxysteroid (17-beta) dehydrogenase 7	Yes
Insc	INSC, spindle orientation adaptor protein	Yes
Kcna10	Potassium voltage-gated channel subfamily A member 10	Yes
Kcnab1	Potassium voltage-gated channel subfamily A member regulatory beta subunit 1	Yes
Lrtm2	Leucine-rich repeats and transmembrane domains 2	Yes
Nek2	NIMA-related kinase 2	Yes
Nsg2	Neuronal vesicle trafficking associated 2	Yes
Ntrk3	Neurotrophic receptor tyrosine kinase 3	-
Ocm/Ocm2	Oncomodulin	Yes
Osbpl11	Oxysterol binding protein-like 11	-
Ptprq	Protein tyrosine phosphatase, receptor type, Q	Yes
Rab3ip	RAB3A interacting protein	Yes
Rasal2	RAS protein activator like 2	-
Tmcc2	Transmembrane and coiled-coil domain family 2	Yes
Vsig10l2	V-Set and immunoglobulin domain containing 10 like 2	Yes
Vwa3a	von Willebrand factor A domain containing 3A	Yes
Xirp2	Xin actin-binding repeat containing 2	Yes

Yes: Gene selectively expressed in HC versus supporting cells, according to literature data (Wu et al., 2013; Burns et al., 2015; Scheffer et al., 2015; Sadler et al., 2020; Wang et al., 2024).

Table 3. Hallmark gene sets identified by GSEA as significantly enriched (FDP q-value < 0.05) in treated vs control samples in the five comparisons in the study.

Comparison	**Mouse/IDPN**	**Rat/IDPN-4wk**	**Rat/IDPN-3wk**	**Rat/IDPN-7wk**	**Rat/STREP**
			(same controls)		
Control vs.:	**30 mM in d.w., 8 wk**	**20 mM in d.w., 4 wk**	**20 mM in d.w., 3 wk**	**20 mM in d.w., 7 wk**	**500 mg/kg per·day , 6 wk**
1st significant gene set (FDR q-value)	Interferon-alpha response (0.000)	Interferon-alpha response (0.000)	MYC _Targets_V1 (0.000)	MYC_Targets_V1 (0.000)	Unfolded protein response (0.000)
2	Interferon-gamma response (0.000)	Interferon-gamma response (0.000)	Interferon-alpha response (0.000)	Interferon-alpha response (0.004)	WNT_beta_catenin signaling(0.048)
3	TNFa signalling via NFkB (0.000)	IL6_JAK_Stat3_signaling (0.001)	IL6_JAK_Stat3 signaling (0.010)	IL6_JAK_Stat3 signaling (0.012)	*TNFa signalling via NFkB (0.051)*
4	Inflammatory response (0.002)	E2F Targets (0.001)	Apical surface (0.020)	E2F Targets (0.014)	*p53 Pathway (0.055)*
5	IL6_JAK_Stat3 signaling (0.003)	MYC_Targets_V1 (0.000)	E2F Targets (0.016)	UV_response_up (0.015)	*MYC _Targets_V1 (0.060)*
6	Allograft rejection (0.007)	MYC_Targets_V2 (0.000)	UV_response_up (0.019)	Apical surface (0.016)	
7	TGF-beta signaling (0.010)	TNFa signalling via NFkB (0.001)	Interferon-gamma response (0.026)	Interferon-gamma response (0.023)	
8	PI3K_Akt_mTOR signaling (0.015)	G2M Checkpoint (0.002)	Apoptosis (0.025)	Apoptosis (0.026)	
9	G2M Checkpoint (0.049)	Apoptosis (0.004)	DNA_Repair (0.027)	p53 Pathway (0.024)	
10		p53 Pathway (0.008)	MYC_Targets_V2 (0.025)	Allograft rejection (0.023)	
11		UV_response_up (0.009)	p53 Pathway (0.023)	MYC_Targets_V2 (0.021)	
12		Allograft rejection (0.024)	Allograft rejection (0.025)	DNA_Repair (0.025)	
13		Hypoxia (0.036)	Xenobiotic metabolism (0.026)	Xenobiotic metabolism (0.025)	
14			Hypoxia 0.032	Reactive_oxigen_species pathway (0.032)	
15			Reactive_oxigen_species pathway (0.033)	Hypoxia (0.032)	
16			WNT_beta_catenin signaling (0.043)	Coagulation (0.043)	
17			Coagulation (0.043)		

FIGURE LEGENDS

Figure 1. Effects of chronic ototoxicity on gene expression in the vestibular sensory epithelium as determined by RNA-seq analysis of control and treated rats or mice (n=3/group). **(A-D):** Principal Component Analysis (PCA) with the 500 most variable genes in four individual experiments, mice treated with IDPN **(A)**, rats treated with streptomycin **(B)**, rats treated with IDPN for 4 weeks **(C)**, and rats treated with IDPN for 3 or 7 weeks **(D)**. Control and treated animals distributed according to PC1. Percent figures are the percent of the total variance accounted for by the component. In the streptomycin experiment, M and F identify male and female rats, respectively. **(E-I):** Expression Heat Maps of the 50 most significantly altered genes in the five control vs treated comparisons emerging from the four experiments in **A-D**. Thus, data are shown comparing IDPN mice **(E)**, streptomycin rats **(F)**, rats treated with IDPN for 4 weeks **(G)**, 3 weeks **(H)**, or 7 weeks **(I)** with the control animals in the experiment. C: control, I: IDPN, S: streptomycin, M: male, F: female.

Figure 2. Volcano plots showing the differentially expressed genes (DEG) in control vs. treated animals according to their log(Padj) and log2-Fold_Change values. Data are shown for IDPN in mice **(A)**, streptomycin in rats **(B)**, and IDPN in rats for 3 weeks **(C)**, 4 weeks **(D)**, and 7 weeks **(E)**. Control animals were the same in the rat/IDPN-3wk and rat/IDPN-7wk comparisons. Labels indicate the 34 genes found downregulated in all five control vs. treated comparisons. N=3/group.

Figure 3. Gene ontology (GO) analyses of the lists of downregulated genes. Graphs show the lists of GO terms significantly enriched in all five control *vs*. treated comparisons: mouse/IDPN, rat/STREP, rat/IDPN-4wk, rat/IDPN-3wk and rat/IDPN-7wk. Broad terms (> 1000 genes) were excluded. The annotated bars show the –log(Padj) values attained by the corresponding term in the rat control vs. streptomycin comparison. **(A):** Biological process (BP). **(B):** Molecular function (MF). **(C):** Cell component (CC).

Figure 4. (A) Venn diagrams of the downregulated and upregulated genes in the five control vs. treated comparisons in the study: mouse/IDPN, rat/STREP, rat/IDPN-4wk, rat/IDPN-3wk and rat/IDPN-7wk. Comparison of the lists of DEGs from each control vs treated comparison identified 34 genes downregulated in rats exposed to streptomycin that were also downregulated in mice and rats exposed to IDPN at any stage of exposure. In contrast, no common gene was identified to be upregulated in all five comparisons. **(B)** Expression heat maps of the 34 genes downregulated in all comparisons.

Figure 5. Common and unique downregulation responses in rat/STREP and rat/IDPN-4wk groups. **(A)** Venn diagram showing the numbers of downregulated genes in one, the other or both experiments. **(B, C, D)** Results of the GO analysis of the three lists of genes downregulated after either treatment (**B**), after streptomycin only (**C**), or after IDPN only (**D**). In all three cases, the original list was reduced by REVIGO analysis of redundancy and elimination of broad terms (> 1,000 genes). All terms identified after reduction are shown in **(B)** and **(C)**; only BP terms are shown in **(D)**.

Figure 6. Comparison of the downregulation responses in the most affected (rat/IDPN-7wk) *vs.* the least affected (rat/IDPN-3wk + rat/STREP groups). **(A)** Venn diagram showing the numbers of downregulated genes in one, the other or both groups of experimental conditions. **(B)** Results of the GO analysis of the 631 genes downregulated in the IDPN-7wk rats but not in the IDPN/3-wk or the STREP rats. Only the BP terms are shown, after reduction of the original list by REVIGO analysis and elimination of broad terms (> 1,000 genes).

Figure 7. Gene ontology (GO) analyses of the lists of upregulated genes. Graph show the list of BP terms significantly enriched in all five control *vs*. treated comparisons: mouse/IDPN, rat/STREP, rat/IDPN-4wk, rat/IDPN-3wk and rat/IDPN-7wk. All terms were broad (> 1000 genes). The annotated bars show the –log(Padj) values attained by the corresponding term in the rat control vs. streptomycin comparison.

Figure 8. Common and unique upregulation responses in rat/STREPTO and rat/IDPN-4wk groups. **(A)** Venn diagram showing the numbers of upregulated genes in one, the other or both experiments. **(B, C, D)** Results of the GO analysis of the three lists of genes upregulated after either treatment (**B**), after streptomycin only (**C**), or after IDPN only (**D**). In all three cases, the original list was reduced by REVIGO analysis of redundancy and elimination of broad terms (> 1,000 genes).

Figure 9. Comparison of the upregulation responses in the most affected (rat/IDPN-7wk) vs. the least affected (rat/IDPN-3wk + rat/STREP) vs. the advanced toxicity (rat/IDPN-4k + mouse/IDPN) groups. **(A)** Venn diagram showing the numbers of upregulated genes in each group of experimental conditions and their intersections. **(B)** Cluster of 53 functionally associated proteins identified by STRING analysis of the list of 245 core genes upregulated in advanced IDPN ototoxicity, defined as genes upregulated in both the rat/IDPN-7wk samples and the rat/IDPN-4wk or the mouse/IDPN samples, but not in the rat/IDPN-3wk or the rat/STREP specimens.

Figure 10. Effect of subchronic ototoxicity on PMCA2, DNER, KCNA10, osteopontin, calretinin, and MYO7A expression in the vestibular sensory epithelium as assessed by immunofluorescent labelling and confocal microscopy. **(A-B)** Images from whole mount utricles of control and treated rats showing the effects of IDPN **(A)** or streptomycin **(B)** on PCMA2 expression in the stereocilia bundles. Images are maximum intensity projections of a stack of 6 planes (2 μm total thickness). **(C)** DNER expression in the neck region of the HCs of the crista in control and streptomycin rats. Images are maximum intensity projections of a stack of 4 planes (1.2 μm total thickness). **(D)** Quantitative analyses of PCMA2 and DNER expression. Bars show mean +/- SEM fluorescence intensity values. Each point is from an individual animal, averaging values from >180 hair bundles (**a and b**) or >400 HCs (c) per animal. *** : p<0.001, ****: p<0.0001, Student's t-test. (**E**) CASPR1 and KCNA10 immunolabelling in a control crista (upper row) and in a crista of a rat exposed to IDPN for 4 weeks (bottom row). In control tissue, both proteins localize in the calyceal junction area. After IDPN, most afferent calyces show a very reduced CASPR1 expression (arrows), while a few retain a high amount of label (asterisk). The corresponding HCs display a marked depletion of KCNA10 label in the calyceal junction, although the non-specific label shown by supporting cells with this antibody (Martin et al., 2024) persisted. **(F)** Quantitative analysis of the effect of chronic IDPN **(a)** and streptomycin **(b)** on the expression of KCNA10 in the calyceal junction area. Bars show mean +/- SEM fluorescence intensity values. Each point is from an individual animal, averaging values from >400 HCs per animal. ** : p<0.01, NS: non significant, Student's t-test. **(G and H).** Ostepontin and MYO7A labels in sections of cristae from control and IDPN-4wk rats. **(I)** Calretinin label in HCII from the periphery of utricles from control and IDPN-4wk rats. **(J)** Quantitative analyses of the effect of chronic IDPN on the expression of osteopontin, MYO7A, and calretinin. Bars show mean +/- SEM fluorescence intensity values. Each data point is from an individual animal, averaging values from 30 HCs per animal. **** : p<0.0001, ns: non significant, Student's t-test. Scale bars = 10 μm in A, B, C, E, and H; 25 μm in G, and I.

Figure 11. Effect of subchronic ototoxicity on *Vsig10l2* expression in HCs. **(A).** Representative images of mRNA expression analysis of *Vsig10l2* and of the control gene *Ppib* by RNA-scope, together with MYO7A immunohistochemistry in the peripheral crista of control (upper row) and IDPN-4wk (lower row) rats. The asterisks and arrows label one example of HCs expressing or not *Visg10l2*, respectively. Note the loss of *Vsig10l2* mRNA label after ototoxicity. Scale bar: 10 μm. **(B).** Representative images of osteopontin, calretinin and VSIG10L2 immunoreactivity in the peripheral utricle of control (upper row) and IDPN-4wk (lower row) rats. Note that VSIG10L2 is expressed in HCI (osteopontin+, asterisks) but not HCII (calretinin+, arrows). Note also the decrease in label for all three antibodies. Scale bar: 10 μm. **(C).** Quantitative analysis of the RNA-scope puncta, comparing *Ppib* and *Vsig10l2* mRNA fluorescence units per HC in the center and periphery of the crista of control and IDPN-4wk rats. **(D).** Quantitative analysis of the anti-VSIG10L2 immunoreactivity, in the striola and periphery regions of the utricle of control and IDPN-4wk rats. In C and D, bars show mean +/- SEM values and each data point is from an individual animal. **: p<0.01, ***: p<0.001, **** : p<0.0001, ns: non significant, Student's t-test.

Figure 12. Effect of subchronic ototoxicity on *Atf3* expression in HCs. **(A).** Representative images of mRNA expression analysis of *Atf3* and of the control gene *Ppib* by RNA-scope, together with MYO7A immunohistochemistry in the peripheral crista of control (upper row) and IDPN-4wk (lower row) rats. Scale bar: 10 μm. **(C).** Quantitative analysis of the RNA-scope puncta, comparing *Ppib* and *Atf3* mRNA fluorescence units per HC in the center and periphery of the crista of control and IDPN-4wk rats. Bars show mean +/- SEM values and each data point is from an individual animal. *: $p<0.05$, ns: non significant, Student's t-test.

Figure 13. Summary of key gene expression responses identified in association with the early steps of HC damage during chronic vestibular toxicity. A single HCI with two supporting cells are represented. HCII do not have calyceal junctions and are affected later during chronic ototoxicity but they finally show similar synaptic uncoupling, ciliary coalescence and extrusion.

Figure 1

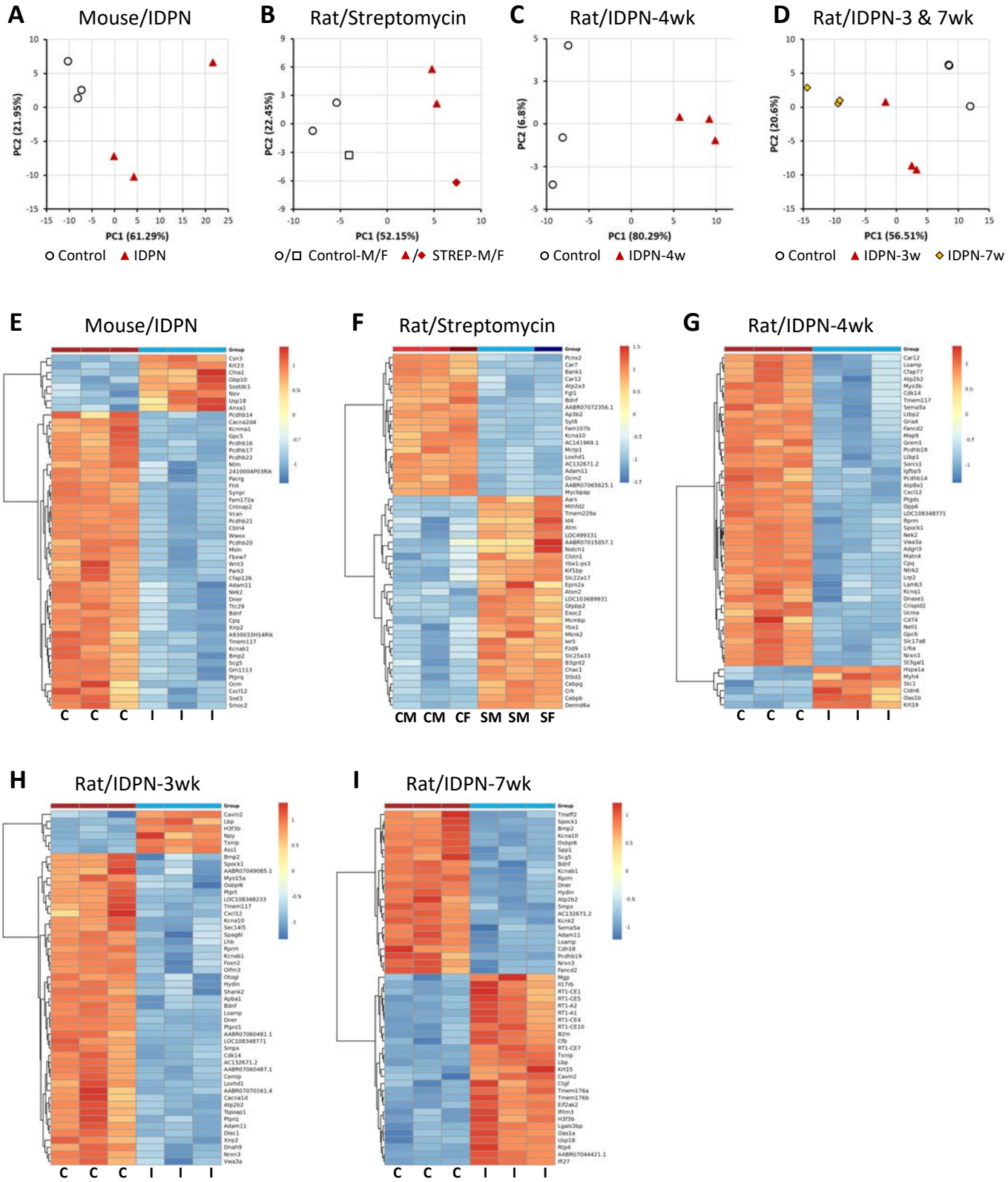
A
Mouse/IDPN
PC2 (21.95%)
PC1 (61.29%)
Control
IDPN
B
Rat/Streptomycin
PC2 (22.45%)
PC1 (52.15%)
Control-M/F
STREP-M/F
C
Rat/IDPN-4wk
PC2 (6.8%)
PC1 (80.29%)
Control
IDPN-4w
D
Rat/IDPN-3 & 7wk
PC2 (20.6%)
PC1 (56.51%)
Control
IDPN-3w
IDPN-7w
E
Mouse/IDPN
C C C I I I
F
Rat/Streptomycin
CM CM CF SM SM SF
G
Rat/IDPN-4wk
C C C I I I
H
Rat/IDPN-3wk
C C C I I I
I
Rat/IDPN-7wk
C C C I I I

Figure 2

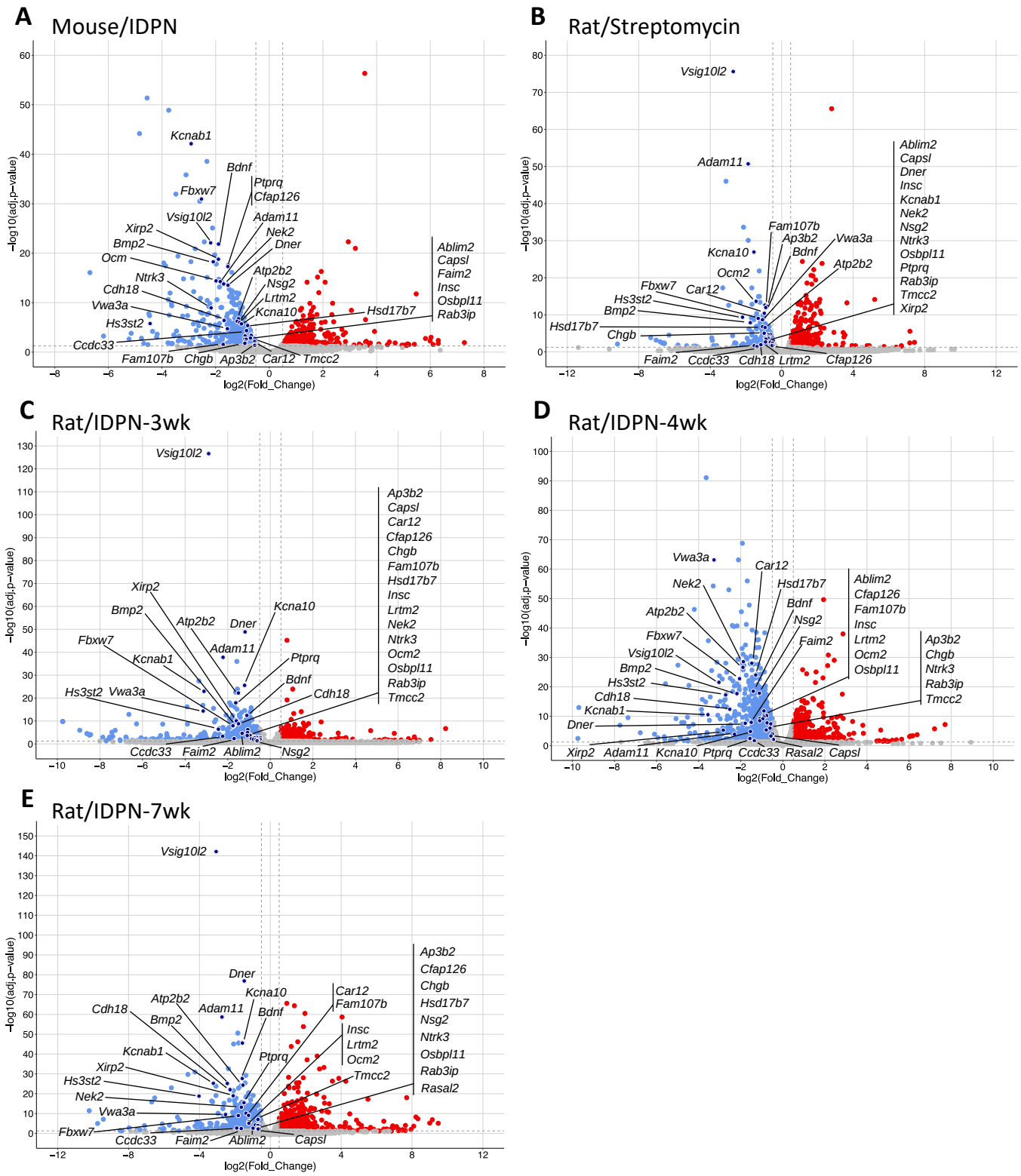
A
Mouse/IDPN
Kcnab1
Bdnf
Ptprq
Cfap126
Fbxw7
Vsig10l2
Adam11
Xirp2
Nek2
Bmp2
Dner
Ocm
Ablim2
Capsl
Faim2
Insc
Osbpl11
Rab3ip
Atp2b2
Ntrk3
Nsg2
Cdh18
Lrtm2
Vwa3a
Kcna10
Hsd17b7
Hs3st2
Ccdc33
Fam107b
Chgb
Ap3b2
Car12
Tmcc2
−log10(adj.p−value)
log2(Fold_Change)
B
Rat/Streptomycin
Vsig10l2
Adam11
Ablim2
Capsl
Dner
Insc
Kcnab1
Nek2
Nsg2
Ntrk3
Osbpl11
Ptprq
Rab3ip
Tmcc2
Xirp2
Fam107b
Ap3b2
Vwa3a
Bdnf
Kcna10
Atp2b2
Ocm2
Fbxw7
Car12
Hs3st2
Bmp2
Hsd17b7
Chgb
Faim2
Ccdc33
Cdh18
Lrtm2
Cfap126
−log10(adj.p−value)
log2(Fold_Change)
C
Rat/IDPN-3wk
Vsig10l2
Ap3b2
Capsl
Car12
Cfap126
Chgb
Fam107b
Hsd17b7
Insc
Lrtm2
Nek2
Ntrk3
Ocm2
Osbpl11
Rab3ip
Tmcc2
Xirp2
Kcna10
Bmp2
Atp2b2
Dner
Fbxw7
Adam11
Kcnab1
Ptprq
Bdnf
Hs3st2
Vwa3a
Cdh18
Ccdc33
Faim2
Ablim2
Nsg2
−log10(adj.p−value)
log2(Fold_Change)
D
Rat/IDPN-4wk
Vwa3a
Car12
Nek2
Hsd17b7
Ablim2
Cfap126
Fam107b
Insc
Lrtm2
Ocm2
Osbpl11
Bdnf
Atp2b2
Nsg2
Faim2
Fbxw7
Vsig10l2
Bmp2
Hs3st2
Cdh18
Kcnab1
Dner
Ap3b2
Chgb
Ntrk3
Rab3ip
Tmcc2
Xirp2
Adam11
Kcna10
Ptprq
Ccdc33
Rasal2
Capsl
−log10(adj.p−value)
log2(Fold_Change)
E
Rat/IDPN-7wk
Vsig10l2
Ap3b2
Cfap126
Chgb
Hsd17b7
Nsg2
Ntrk3
Osbpl11
Rab3ip
Rasal2
Dner
Kcna10
Car12
Fam107b
Atp2b2
Cdh18
Adam11
Bdnf
Bmp2
Insc
Lrtm2
Ocm2
Kcnab1
Ptprq
Xirp2
Tmcc2
Hs3st2
Nek2
Vwa3a
Fbxw7
Ccdc33
Faim2
Ablim2
Capsl
−log10(adj.p−value)
log2(Fold_Change)

Figure 3

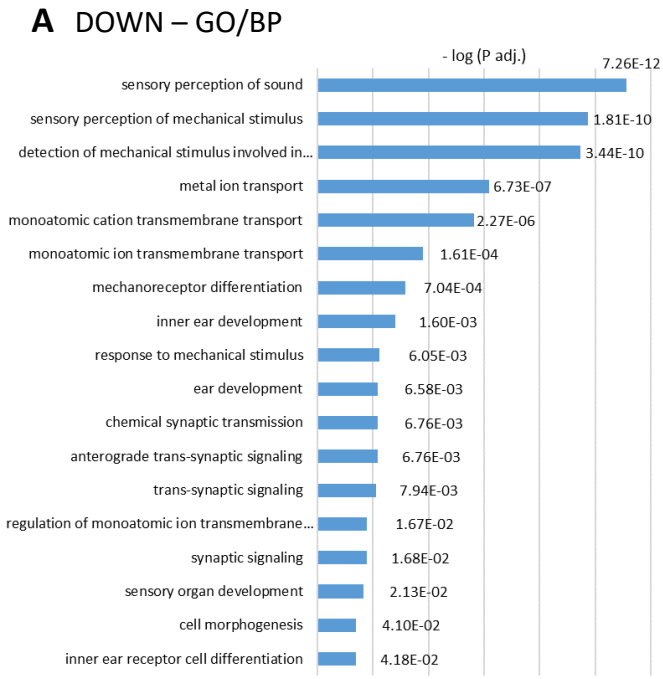
A DOWN – GO/BP
- log (P adj.)
sensory perception of sound
7.26E-12
sensory perception of mechanical stimulus
1.81E-10
detection of mechanical stimulus involved in...
3.44E-10
metal ion transport
6.73E-07
monoatomic cation transmembrane transport
2.27E-06
monoatomic ion transmembrane transport
1.61E-04
mechanoreceptor differentiation
7.04E-04
inner ear development
1.60E-03
response to mechanical stimulus
6.05E-03
ear development
6.58E-03
chemical synaptic transmission
6.76E-03
anterograde trans-synaptic signaling
6.76E-03
trans-synaptic signaling
7.94E-03
regulation of monoatomic ion transmembrane...
1.67E-02
synaptic signaling
1.68E-02
sensory organ development
2.13E-02
cell morphogenesis
4.10E-02
inner ear receptor cell differentiation
4.18E-02

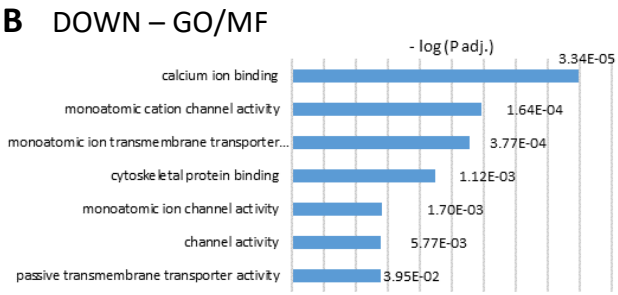
B DOWN – GO/MF
- log (P adj.)
calcium ion binding
3.34E-05
monoatomic cation channel activity
1.64E-04
monoatomic ion transmembrane transporter...
3.77E-04
cytoskeletal protein binding
1.12E-03
monoatomic ion channel activity
1.70E-03
channel activity
5.77E-03
passive transmembrane transporter activity
3.95E-02

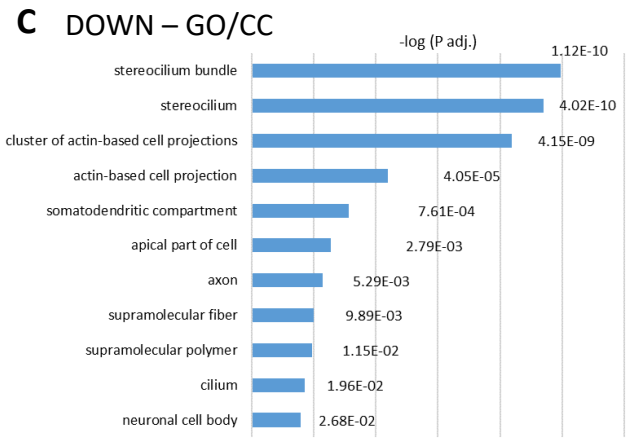
C DOWN – GO/CC
-log (P adj.)
stereocilium bundle
1.12E-10
stereocilium
4.02E-10
cluster of actin-based cell projections
4.15E-09
actin-based cell projection
4.05E-05
somatodendritic compartment
7.61E-04
apical part of cell
2.79E-03
axon
5.29E-03
supramolecular fiber
9.89E-03
supramolecular polymer
1.15E-02
cilium
1.96E-02
neuronal cell body
2.68E-02

Figure 4

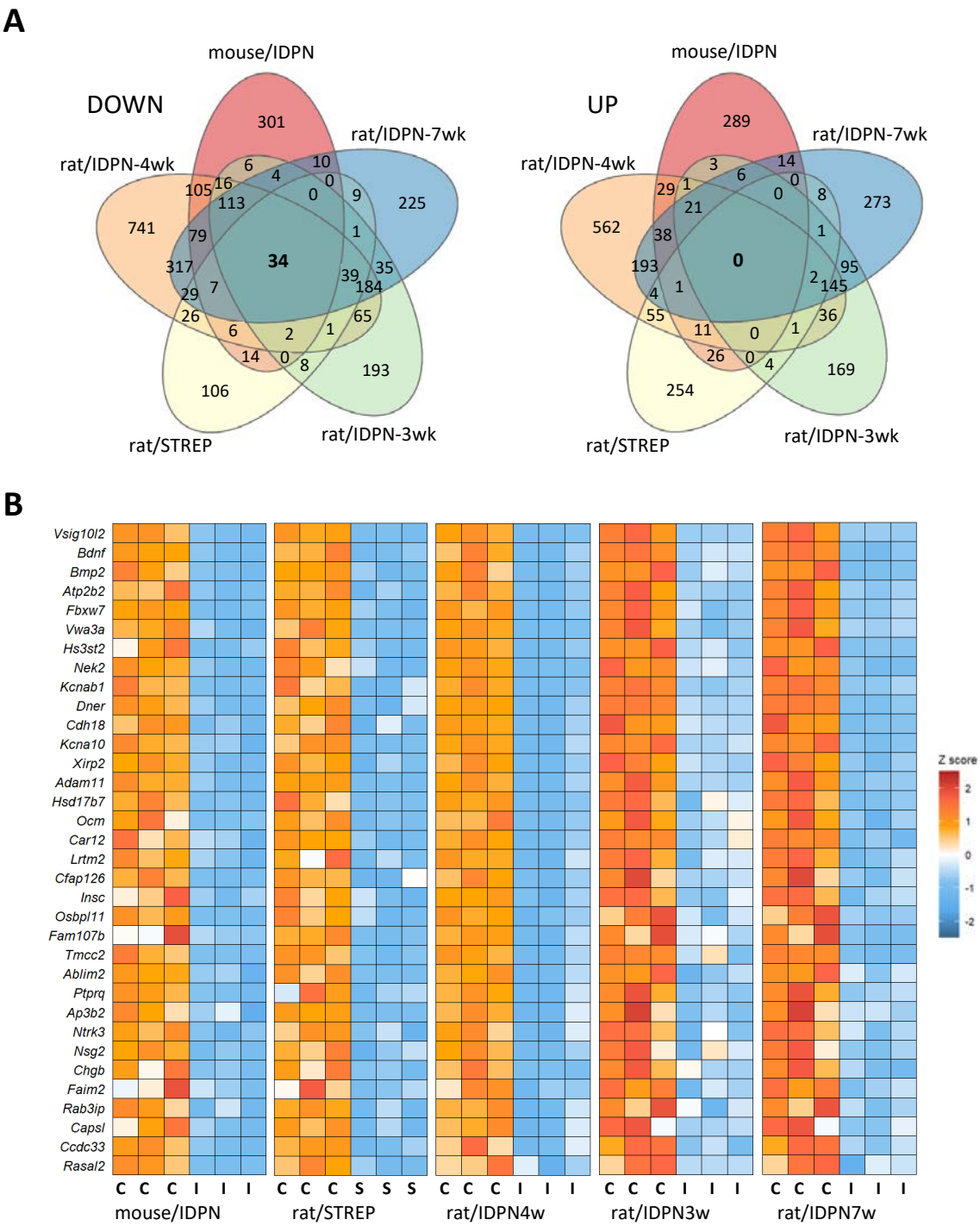
A
DOWN
mouse/IDPN
rat/IDPN-7wk
rat/IDPN-4wk
rat/STREP
rat/IDPN-3wk
301
225
741
106
193
34
UP
mouse/IDPN
rat/IDPN-7wk
rat/IDPN-4wk
rat/STREP
rat/IDPN-3wk
289
273
562
254
169
0
B
Vsig10l2
Bdnf
Bmp2
Atp2b2
Fbxw7
Vwa3a
Hs3st2
Nek2
Kcnab1
Dner
Cdh18
Kcna10
Xirp2
Adam11
Hsd17b7
Ocm
Car12
Lrtm2
Cfap126
Insc
Osbpl11
Fam107b
Tmcc2
Ablim2
Ptprq
Ap3b2
Ntrk3
Nsg2
Chgb
Faim2
Rab3ip
Capsl
Ccdc33
Rasal2
C C C I I I
mouse/IDPN
C C C S S S
rat/STREP
C C C I I I
rat/IDPN4w
C C C I I I
rat/IDPN3w
C C C I I I
rat/IDPN7w
Z score
2
1
0
-1
-2

Figure 5

A
DOWN
rat/IDPN-4wk
1620
142
138
rat/STREP
B
Common
BIOLOGICAL PROCESS
sensory perception of sound
mechanoreceptor differentiation
CELLULAR COMPONENT
stereocilium bundle
cluster of actin-based cell projections
actin-based cell projection
cation channel complex
apical part of cell
-log(p value)
Number of genes
MOLECULAR FUNCTION
calcium-dependent ATPase activity
calcium ion binding
C
STREPTOMYCIN only
BIOLOGICAL PROCESS
detection of mechanical stimulus. involved in sensory perception of sound
sodium ion transmembrane transport
MOLECULAR FUNCTION
sulfur compound binding
metal ion transmembr. transporter activ.
Enrichment
D
IDPN only
BIOLOGICAL PROCESS
reflex
membrane repolarization
cell-cell adhesion via plasma-membrane adhesion molecules
locomotory behavior
sensory perception of sound
regulation of synapse structure or activity
regulation of cell-substrate adhesion
inner ear development
behavior
chemotaxis
synapse organization
microtubule-based transport
extracellular matrix organization
extracellular structure organization
external encapsulating structure organization
neuron projection development
microtubule-based movement
modulation of chemical synaptic transmission
regulation of transporter activity
cell morphogenesis
cell junction organization
positive regulation of cell migration
reg. of plasma memb. bounded cell project. organiz.
regulation of nervous system development
regulation of membrane potential
tissue migration
sensory organ development
chemical synaptic transmission
response to metal ion
regulation of monoatomic ion transport
sensory system development
monoatomic ion transmembrane transport
blood circulation
regulation of locomotion
monoatomic ion homeostasis
regulation of cell adhesion
export from cell
transmemb. recep. prot. tyr. kinase sign. pathway
head development
actin filament-based process
vasculature development
supramolecular fiber organization
microtubule-based process
tube development
secretion
actin cytoskeleton organization
positive regulation of phosphorylation
response to organonitrogen compound
response to nitrogen compound
response to abiotic stimulus
Number of genes
-log(p value)
Enrichment

Fig 6

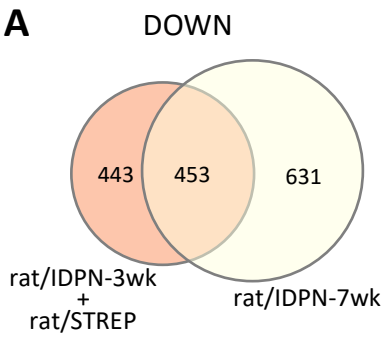
A
DOWN
443
453
631
rat/IDPN-3wk
+
rat/STREP
rat/IDPN-7wk

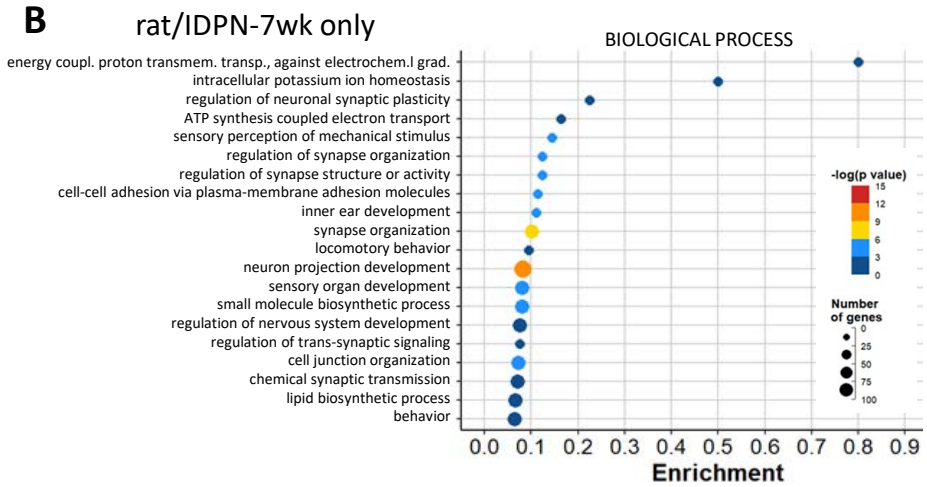
B
rat/IDPN-7wk only
BIOLOGICAL PROCESS
energy coupl. proton transmem. transp., against electrochem.l grad.
intracellular potassium ion homeostasis
regulation of neuronal synaptic plasticity
ATP synthesis coupled electron transport
sensory perception of mechanical stimulus
regulation of synapse organization
regulation of synapse structure or activity
cell-cell adhesion via plasma-membrane adhesion molecules
inner ear development
synapse organization
locomotory behavior
neuron projection development
sensory organ development
small molecule biosynthetic process
regulation of nervous system development
regulation of trans-synaptic signaling
cell junction organization
chemical synaptic transmission
lipid biosynthetic process
behavior
-log(p value)
15
12
9
6
3
0
Number of genes
0
25
50
75
100
0.0 0.1 0.2 0.3 0.4 0.5 0.6 0.7 0.8 0.9
Enrichment

Figure 7

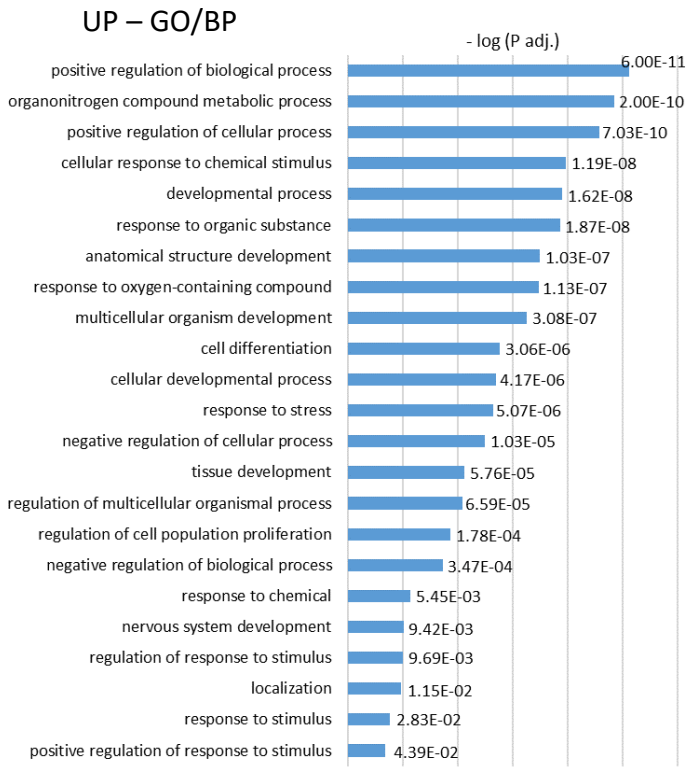
UP – GO/BP
- log (P adj.)
positive regulation of biological process
6.00E-11
organonitrogen compound metabolic process
2.00E-10
positive regulation of cellular process
7.03E-10
cellular response to chemical stimulus
1.19E-08
developmental process
1.62E-08
response to organic substance
1.87E-08
anatomical structure development
1.03E-07
response to oxygen-containing compound
1.13E-07
multicellular organism development
3.08E-07
cell differentiation
3.06E-06
cellular developmental process
4.17E-06
response to stress
5.07E-06
negative regulation of cellular process
1.03E-05
tissue development
5.76E-05
regulation of multicellular organismal process
6.59E-05
regulation of cell population proliferation
1.78E-04
negative regulation of biological process
3.47E-04
response to chemical
5.45E-03
nervous system development
9.42E-03
regulation of response to stimulus
9.69E-03
localization
1.15E-02
response to stimulus
2.83E-02
positive regulation of response to stimulus
4.39E-02

Figure 8

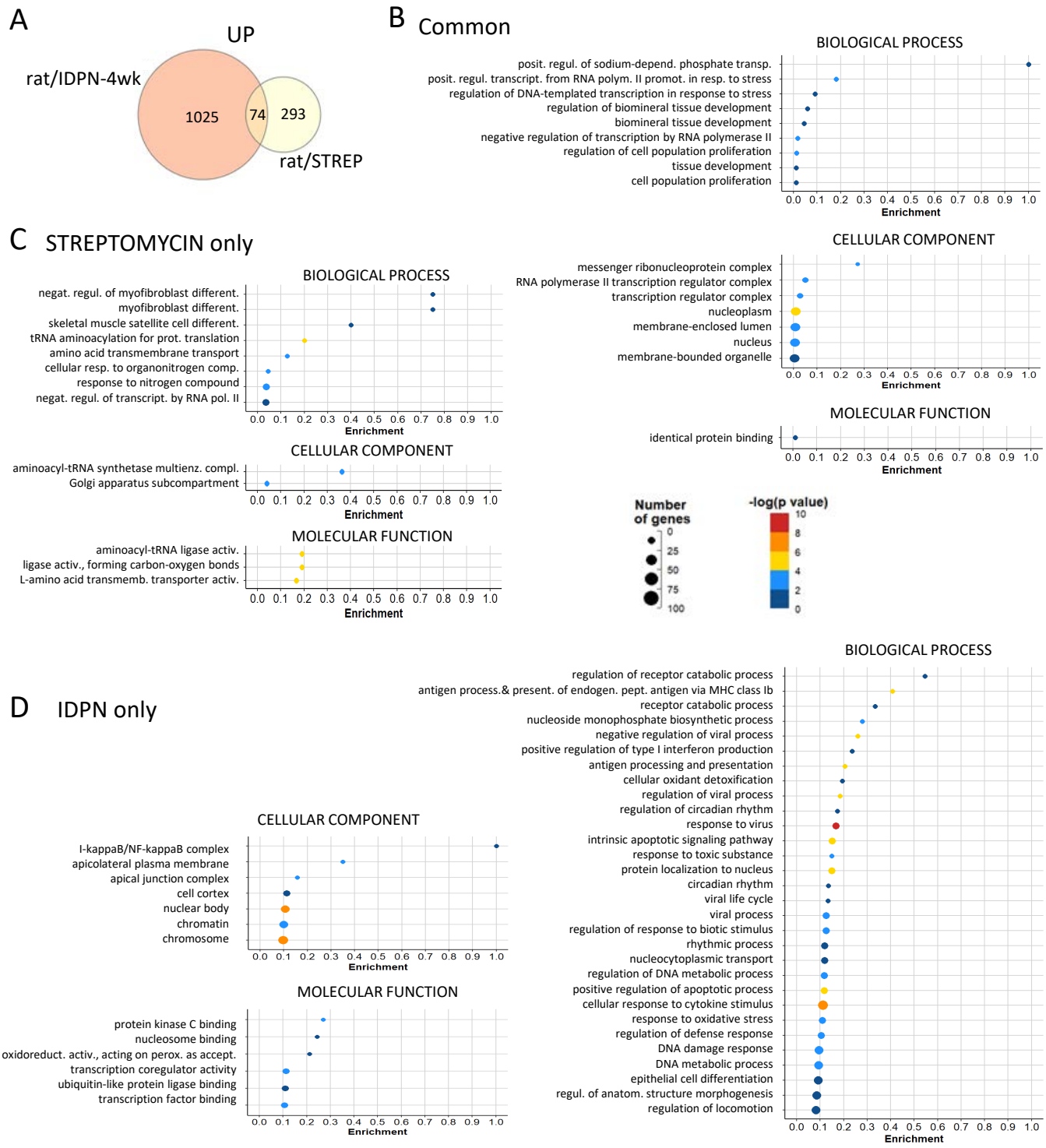
A
UP
rat/IDPN-4wk
1025
74
293
rat/STREP
B Common
BIOLOGICAL PROCESS
posit. regul. of sodium-depend. phosphate transp.
posit. regul. transcript. from RNA polym. II promot. in resp. to stress
regulation of DNA-templated transcription in response to stress
regulation of biomineral tissue development
biomineral tissue development
negative regulation of transcription by RNA polymerase II
regulation of cell population proliferation
tissue development
cell population proliferation
0.0 0.1 0.2 0.3 0.4 0.5 0.6 0.7 0.8 0.9 1.0
Enrichment
C STREPTOMYCIN only
BIOLOGICAL PROCESS
negat. regul. of myofibroblast different.
myofibroblast different.
skeletal muscle satellite cell different.
tRNA aminoacylation for prot. translation
amino acid transmembrane transport
cellular resp. to organonitrogen comp.
response to nitrogen compound
negat. regul. of transcript. by RNA pol. II
0.0 0.1 0.2 0.3 0.4 0.5 0.6 0.7 0.8 0.9 1.0
Enrichment
CELLULAR COMPONENT
aminoacyl-tRNA synthetase multienz. compl.
Golgi apparatus subcompartment
0.0 0.1 0.2 0.3 0.4 0.5 0.6 0.7 0.8 0.9 1.0
Enrichment
MOLECULAR FUNCTION
aminoacyl-tRNA ligase activ.
ligase activ., forming carbon-oxygen bonds
L-amino acid transmemb. transporter activ.
0.0 0.1 0.2 0.3 0.4 0.5 0.6 0.7 0.8 0.9 1.0
Enrichment
CELLULAR COMPONENT
messenger ribonucleoprotein complex
RNA polymerase II transcription regulator complex
transcription regulator complex
nucleoplasm
membrane-enclosed lumen
nucleus
membrane-bounded organelle
0.0 0.1 0.2 0.3 0.4 0.5 0.6 0.7 0.8 0.9 1.0
Enrichment
MOLECULAR FUNCTION
identical protein binding
0.0 0.1 0.2 0.3 0.4 0.5 0.6 0.7 0.8 0.9 1.0
Enrichment
Number of genes
0
25
50
75
100
-log(p value)
10
8
6
4
2
0
D IDPN only
BIOLOGICAL PROCESS
regulation of receptor catabolic process
antigen process.& present. of endogen. pept. antigen via MHC class Ib
receptor catabolic process
nucleoside monophosphate biosynthetic process
negative regulation of viral process
positive regulation of type I interferon production
antigen processing and presentation
cellular oxidant detoxification
regulation of viral process
regulation of circadian rhythm
response to virus
intrinsic apoptotic signaling pathway
response to toxic substance
protein localization to nucleus
circadian rhythm
viral life cycle
viral process
regulation of response to biotic stimulus
rhythmic process
nucleocytoplasmic transport
regulation of DNA metabolic process
positive regulation of apoptotic process
cellular response to cytokine stimulus
response to oxidative stress
regulation of defense response
DNA damage response
DNA metabolic process
epithelial cell differentiation
regul. of anatom. structure morphogenesis
regulation of locomotion
0.0 0.1 0.2 0.3 0.4 0.5 0.6 0.7 0.8 0.9 1.0
Enrichment
CELLULAR COMPONENT
I-kappaB/NF-kappaB complex
apicolateral plasma membrane
apical junction complex
cell cortex
nuclear body
chromatin
chromosome
0.0 0.1 0.2 0.3 0.4 0.5 0.6 0.7 0.8 0.9 1.0
Enrichment
MOLECULAR FUNCTION
protein kinase C binding
nucleosome binding
oxidoreduct. activ., acting on perox. as accept.
transcription coregulator activity
ubiquitin-like protein ligase binding
transcription factor binding
0.0 0.1 0.2 0.3 0.4 0.5 0.6 0.7 0.8 0.9 1.0
Enrichment

Figure 9

A

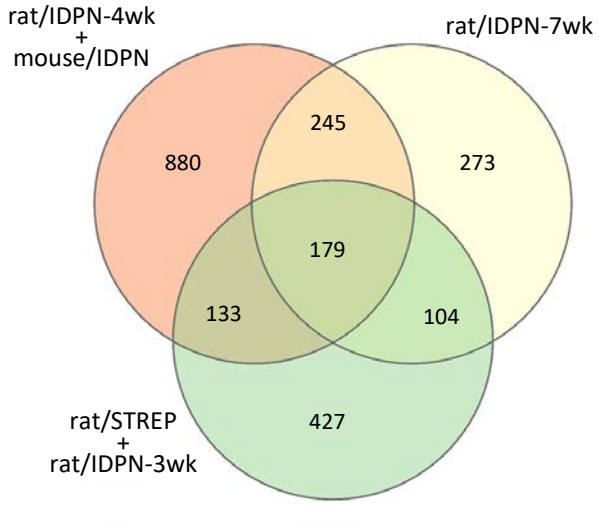
rat/IDPN-4wk
+
mouse/IDPN
rat/IDPN-7wk
880
245
273
179
133
104
427
rat/STREP
+
rat/IDPN-3wk

B

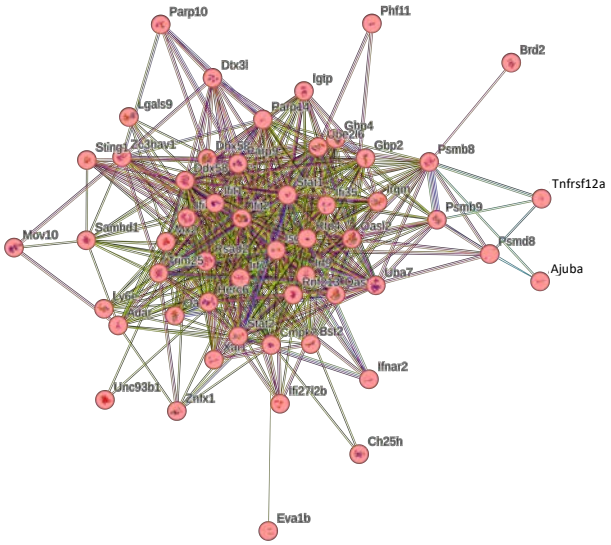
Parp10
Phf11
Brd2
Dtx3l
Igtp
Lgals9
Parp9
Gbp4
Gbp2
Psmb8
Sting1
Zc3hav1
Tnfrsf12a
Psmb9
Mov10
Samhd1
Psmd8
Ajuba
Uba7
Bst2
Ifnar2
Unc93b1
Znfx1
Ifi27l2b
Ch25h
Eva1b

Figure 10

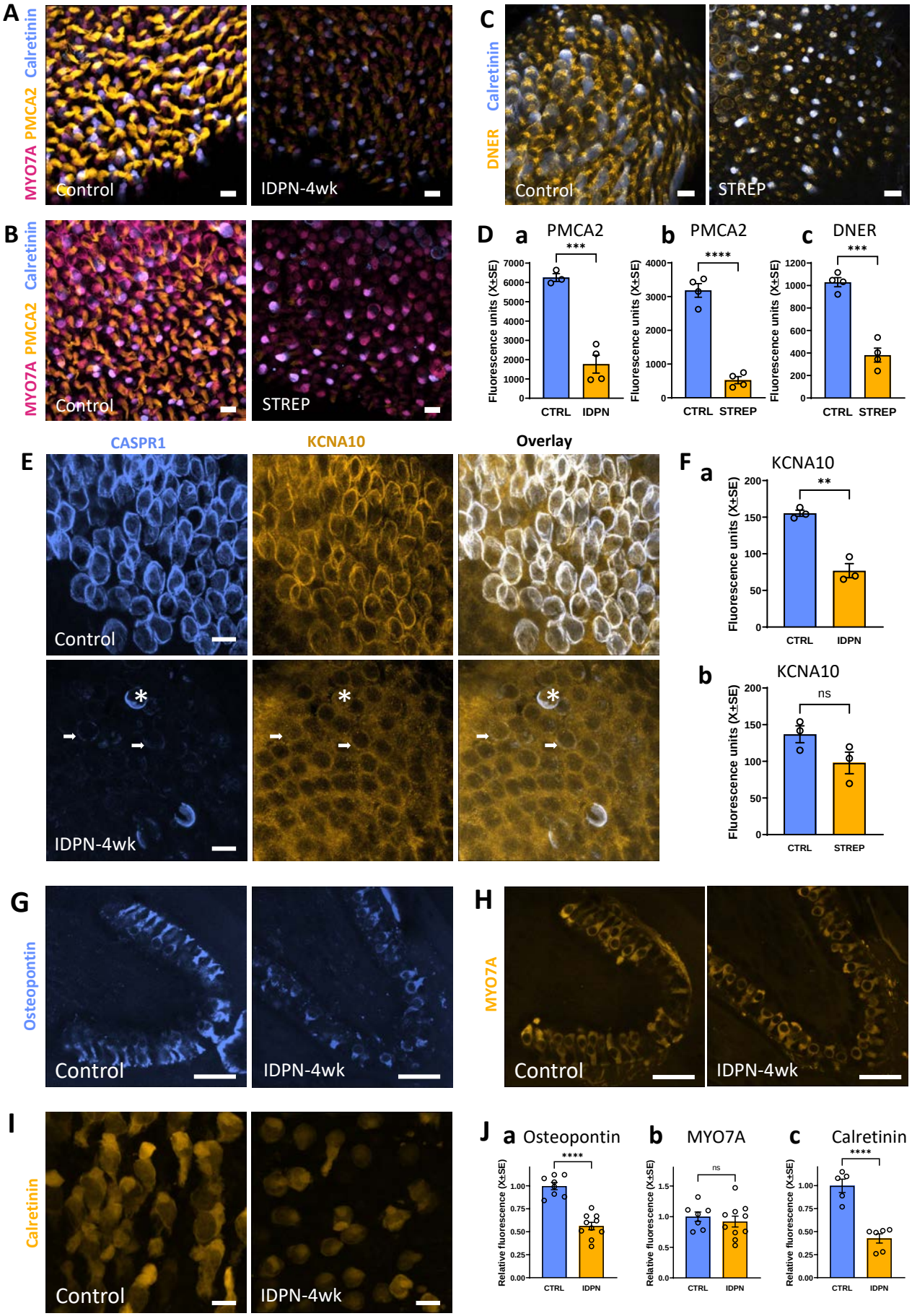
A
MYO7A PMCA2 Calretinin
Control
IDPN-4wk
B
MYO7A PMCA2 Calretinin
Control
STREP
C
DNER Calretinin
Control
STREP
D
a PMCA2
b PMCA2
c DNER
Fluorescence units (X±SE)
CTRL IDPN
CTRL STREP
E
CASPR1
KCNA10
Overlay
Control
IDPN-4wk
F
a KCNA10
b KCNA10
ns
G
Osteopontin
Control
IDPN-4wk
H
MYO7A
Control
IDPN-4wk
I
Calretinin
Control
IDPN-4wk
J
a Osteopontin
b MYO7A
c Calretinin
Relative fluorescence (X±SE)
CTRL IDPN

Figure 11

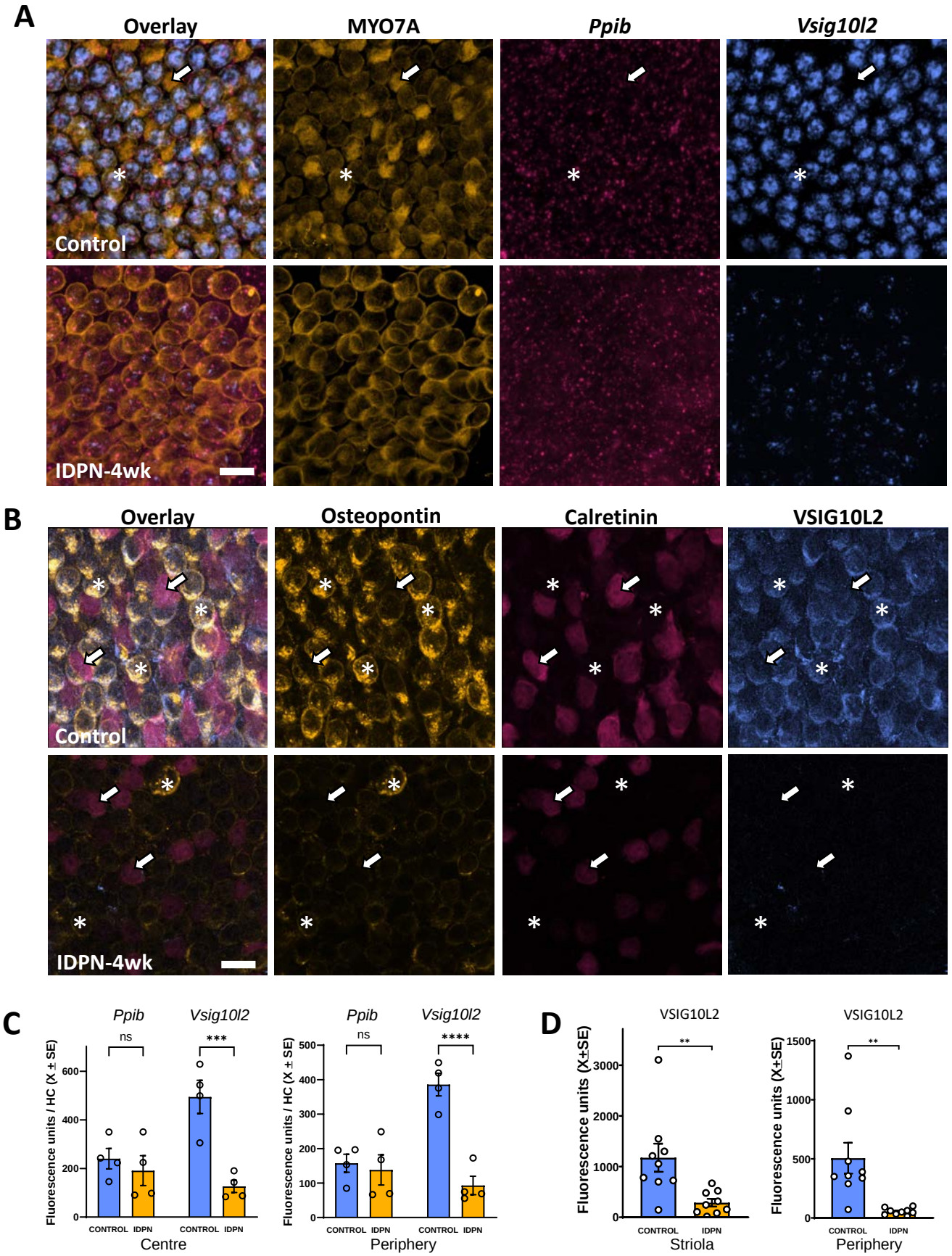
A
Overlay
MYO7A
Ppib
Vsig10l2
Control
IDPN-4wk
B
Overlay
Osteopontin
Calretinin
VSIG10L2
Control
IDPN-4wk
C
Ppib
Vsig10l2
ns
***
Fluorescence units / HC (X ± SE)
CONTROL
IDPN
Centre
Ppib
Vsig10l2
ns
****
Fluorescence units / HC (X ± SE)
CONTROL
IDPN
Periphery
D
VSIG10L2
**
Fluorescence units (X±SE)
CONTROL
IDPN
Striola
VSIG10L2
**
Fluorescence units (X±SE)
CONTROL
IDPN
Periphery

Figure 12

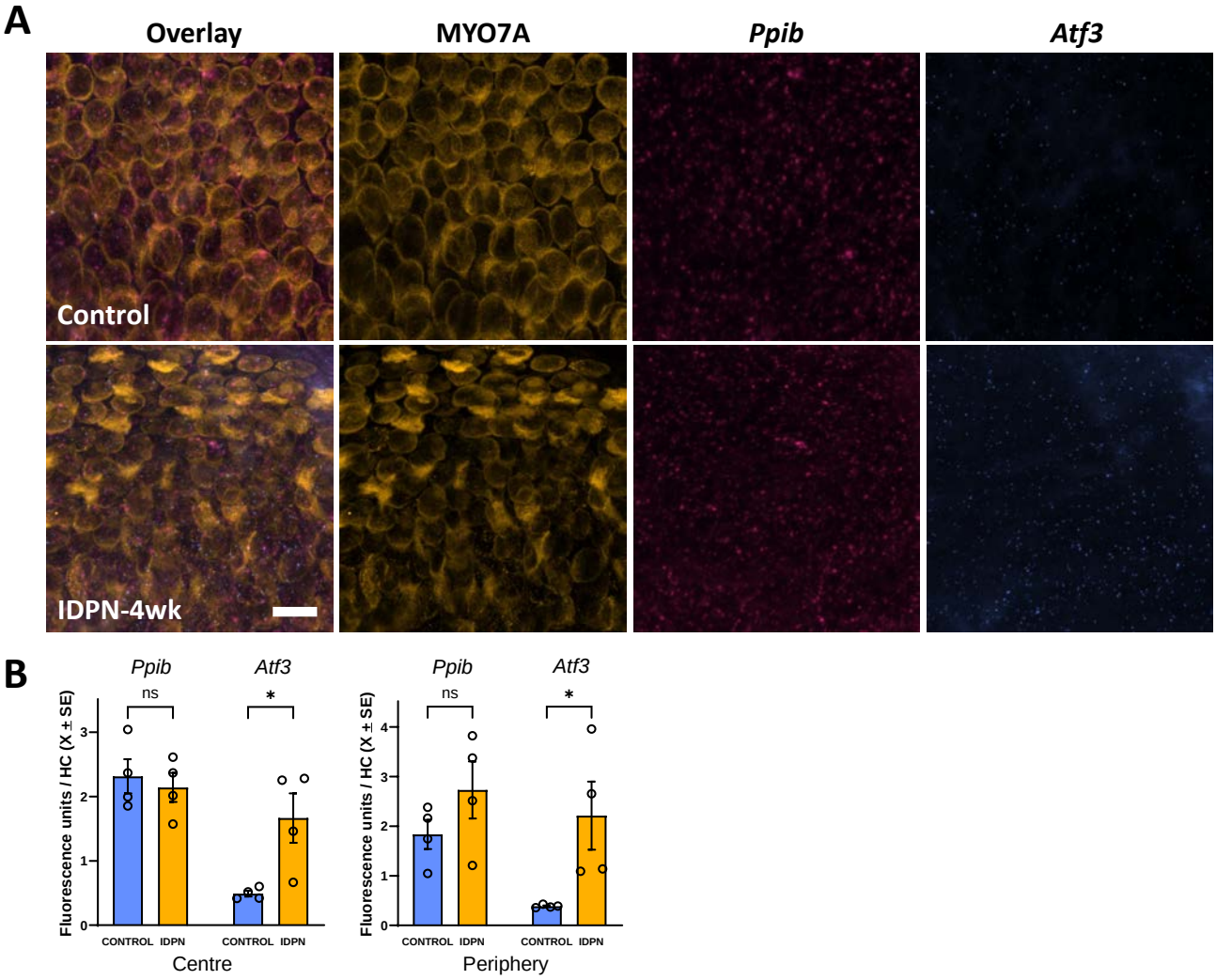
A
Overlay
MYO7A
Ppib
Atf3
Control
IDPN-4wk
B
Ppib
Atf3
ns
*
Fluorescence units / HC (X ± SE)
CONTROL
IDPN
Centre
Periphery

Figure 13

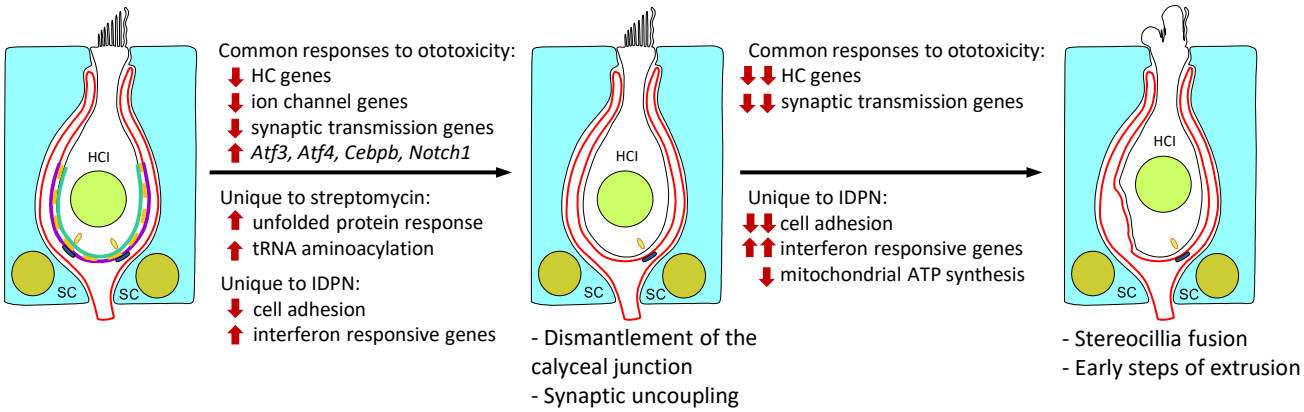
HCI
SC
SC
Common responses to ototoxicity:
HC genes
ion channel genes
synaptic transmission genes
Atf3, Atf4, Cebpb, Notch1
Unique to streptomycin:
unfolded protein response
tRNA aminoacylation
Unique to IDPN:
cell adhesion
interferon responsive genes
HCI
SC
SC
- Dismantlement of the calyceal junction
- Synaptic uncoupling
Common responses to ototoxicity:
HC genes
synaptic transmission genes
Unique to IDPN:
cell adhesion
interferon responsive genes
mitochondrial ATP synthesis
HCI
SC
SC
- Stereocillia fusion
- Early steps of extrusion